

Mela Schabrich

Coupled dynamic analysis of a floating dock system for installation of a spar wind turbine

Master's thesis in Marine Technology (MTMART)

Supervisor: Zhen Gao

June 2019

Mela Schabrich

Coupled dynamic analysis of a floating dock system for installation of a spar wind turbine

Master's thesis in Marine Technology
Supervisor: Zhen Gao
June 2019

Norwegian University of Science and Technology
Faculty of Engineering
Department of Marine Technology



Abstract

A floating dock concept has been developed to assemble spar floating wind turbines near the offshore wind farm site. The concept comprises a floating dock that is moored on site with chains to the sea bed. The dock is shaped as a vertical tube giving space to install the wind turbines in its center and storing the components dryly on the top of its sides. It gives also space for cranes, living accommodation, offices and a landing platform. The main motivation for this concept is that the turbines can be completed in the floating dock close to the site and not at a shipyard from where they have to be towed to the site.

At the time of the thesis, the conceptual design of the floating dock has already been validated and the dimensions have been optimized in regards to performance and cost. Also a series of model tests and a few numerical motion analyses have been separately performed. The purpose of this thesis is to establish a numerical model which coincide with the results of conducted model tests and to examine the behaviour of the dock in its operational mode. Two different numerical modelling approaches are established. The hydrodynamic problem is hereby solved in WAMIT, a program that analyzes the interaction between ocean waves and offshore structures. Further modifications and simulations in time domain are run in SIMA, a workbench that analyses marine operations and floating systems. The results of the simulations, run under regular wave conditions, are compared and modified in regards to the model tests results. The comparison is hereby made based on the non-dimensional response amplitude operator (RAO) which is the transfer function between the wave amplitude and the dock motion.

The first approach turned out to be inadequate while the second approach proven to display reality sufficiently. So that in addition to the regular wave conditions, irregular wave conditions and decay tests are conducted for the second approach. Natural periods, power spectra, maximum motions and velocities are discussed and evaluated. Based on the evaluation, it can be concluded that with a modified mooring system the results should realistically describe the behaviour of the structure in its operational mode.

In closing, the most important points of the thesis are summed up and recommendations for future work are given. A recommendable next step is hereby certainly to replace the current mooring system, which is based on the mooring system of the model tests, with the mooring system of the actual dock.

Preface

This thesis is submitted to the Norwegian University of Science and Technology (NTNU) as partial fulfillment of the requirements for the degree of master. It has been performed at the Department of Marine Technology, NTNU, Trondheim, with Professor Zhen Gao as main supervisor and with support from Jingzhe Jin, Maël Moreau and Zhiyu Jiang. The supports are gratefully acknowledged.

Contents

Abstract	i
Preface	ii
Table of Contents	iv
List of Tables	v
List of Figures	viii
Abbreviations	ix
1 Introduction	1
1.1 Background	1
1.2 Motivation	5
1.2.1 Norway Hywind Demo	5
1.2.2 Scotland Hywind Park	5
1.2.3 Resulting Challenges	7
1.3 Main Concept	8
2 Theory	15
2.1 Sloshing Effects	15
2.2 Coupling Effects	17
2.3 Response Amplitude Operator	19
3 Numerical Modelling	21
3.1 Previous Work	21
3.2 First Approach	24
3.2.1 Introduction to WAMIT model	24
3.2.2 Calibration of WAMIT model	26
3.2.3 Input to SIMA	30

3.2.4	Modification in SIMA	31
3.3	Second Approach	33
3.3.1	Introduction to WAMIT model	33
3.3.2	Calibration of WAMIT model	34
3.3.3	Input to SIMA	34
3.3.4	Modification in SIMA	35
4	Analysis	37
4.1	Regular Wave Conditions	37
4.1.1	Time series	37
4.1.2	Response Amplitude Operators	40
4.2	Decay Tests	43
4.3	Irregular Wave Conditions	45
5	Discussion	51
5.1	Modelling Approach	51
5.2	Results of Analyses	53
6	Conclusion	55
6.1	Summary	55
6.2	Recommendation for future work	56
	Bibliography	59
	Appendix	61

List of Tables

3.1	Design variables with latest values	22
3.2	Design variables in model test (Set 2)	24
3.3	Froude scaling table [22]	26
3.4	Set drag coefficients	33
3.5	DOFs in WAMIT	34
3.6	Corresponding DOFs in SIMA	35
4.1	Maximum motion	48
4.2	Maximum velocity	48
4.3	Positioning force	49
6.1	Model tests - Wave periods	63
6.2	Model tests - Wave periods and heights in full scale	65
6.3	Results for wave condition: $H_s=2m$, $T_p=9s$	72
6.4	Results for wave condition: $H_s=2m$, $T_p=13s$	72
6.5	Results for wave condition: $H_s=3m$, $T_p=9s$	73
6.6	Results for wave condition: $H_s=3m$, $T_p=13s$	73
6.7	Results for wave condition: $H_s=1.1m$, $T_p=14.2s$	73

List of Figures

1.1	Jacket OWT [4]	2
1.2	Monopile OWT [4]	2
1.3	Gravity-based OWT [4]	2
1.4	Spar OWT [6]	3
1.5	Semi-submersible OWT [6]	4
1.6	TLP OWT [6]	4
1.7	Norway Hywind Demo [7]	5
1.8	Transportation of Hywind turbines [13]	6
1.9	Hywind Scotland - Illustration Equinor [10]	7
1.10	Lift operation Hywind Scotland [16]	8
1.11	Main concept [17]	9
1.12	Different installation methods of turbine components [5]	10
2.1	Spectral problem	16
2.2	Viscous damping	17
2.3	RAO variables in surge	19
3.1	Design variables in operational condition	22
3.2	Model test	23
3.3	Dock meshing	26
3.4	Moment of inertia - Variables	28
3.5	Mooring system in top view	29
3.6	Mooring system in side view	29
3.7	Formation of slender elements	32
3.8	Cylinder with moonpool - Example 17a [21]	33
3.9	Model in SIMA	36
4.1	Dock motion in pitch at wave period of 17s	38
4.2	Dock motion in surge at wave period of 9s	38
4.3	Dock motion in heave at wave period of 13s	38

4.4	Dock motion in surge at wave period of 21s	39
4.5	Dock motion in pitch at wave period of 23s	39
4.6	Dock motion in pitch at wave period of 15s	39
4.7	Dock motion in surge at wave period of 21s	40
4.8	Dock motion in heave at wave period of 9s	40
4.9	RAOs in surge for the first and second approach	41
4.10	RAOs in heave for the first and second approach	41
4.11	RAOs in pitch for the first and second approach	42
4.12	Decay test in surge	44
4.13	Decay test in heave	44
4.14	Decay test in pitch	45
4.15	Operational mode - Wave spectrum	46
4.16	Operational mode - Response spectrum in surge	46
4.17	Operational mode - Response spectrum in heave	46
4.18	Operational mode - Response spectrum in pitch	46
4.19	Survival mode - Wave spectrum	47
4.20	Survival mode - Response spectrum in surge	47
4.21	Survival mode - Response spectrum in heave	47
4.22	Survival mode - Response spectrum in pitch	47
5.1	RAOs in surge for different C_{Ds}	52
5.2	RAOs in heave for different C_{Ds}	52
5.3	RAOs in pitch for different C_{Ds}	52
6.1	Mooring system of Zhiyu Jiang's model [25]	57
6.2	Design constraints [26]	62
6.3	Shallow dock constraints [26]	62

Abbreviations

CoG	=	Center of Gravity
DOF	=	Degree of Freedom
HLV	=	Heavy Lift Vessel
KC	=	Keulegan Carpenter
OWT	=	Offshore Wind Turbine
RAO	=	Response Amplitude Operator
TLP	=	Tension Leg Platform
VIM	=	Vortex Induced Motion
WT	=	Wind Turbine

Introduction

This master thesis deals with the calibration of a floating dock model in the computer program SIMA. The floating dock is designed for installing offshore spar wind turbines all around the world. The calibration is mainly based on the results of model tests conducted by Maël Moreau and his supervisor Trygve Kristiansen in towing tank III of Sintef Ocean, Trondheim. To get a better understanding of why this thesis is germane, the following sections provide an overview of the background, the motivation and the main concept of this project.

1.1 Background

2010 the worldwide energy consumption was 8,677 Mtoe. In 2015, it increased to 9,384 Mtoe. This is a rise of around 7.5% in only ten years. The consumption of energy increases steadily every year. [1] Meanwhile due to climate change, the urgency to switch to green energy sources arose. Green energy sources can be the sun, wind or water in terms of waves and current. The most utilized green energy source is currently the sun [1]. But also wind energy plays an ever increasing role. By the end of 2017, the overall capacity of wind turbines (WT) installed worldwide reached around 514 GW [2]. Hereby 96.3% was produced by onshore and 3.7% by offshore wind parks [2]. Why is still so much wind energy produced onshore? Land is only limited available. The world population increases. More space for living and food production is needed. In addition to that, there is a lot of acoustical and visual impacts on humans when wind parks operate onshore. When operated offshore, the parks do not effect humans. Also the transportation is simpler and most important, larger-scaled turbines can be used. [3] All these advantages speak in favour of offshore wind parks. So why are there not more of them? One of the reasons is the limited coastal area suitable for the installation of bottom fixed wind turbines. There are three types of bottom fixed WTs: jackets, monopiles and gravity based WTs.

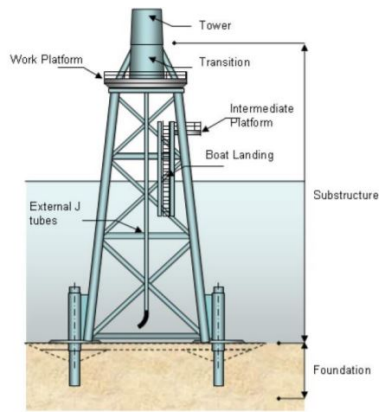


Figure 1.1: Jacket OWT [4]

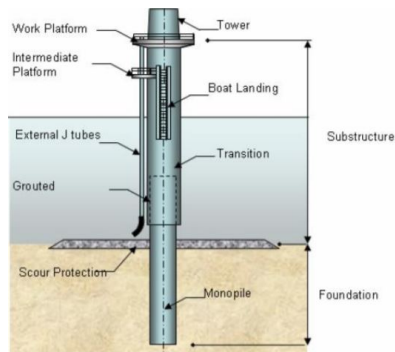


Figure 1.2: Monopile OWT [4]

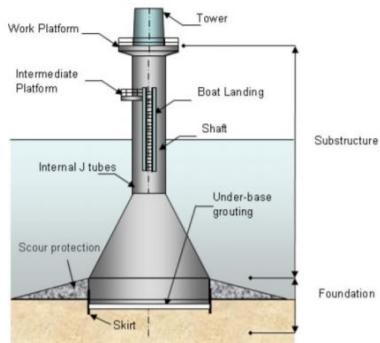


Figure 1.3: Gravity-based OWT [4]

Monopiles are applicable in water depths up to 40 m with a sea floor soft enough to hammer the pile into the ground [5] (see Figure 1.2). Gravity based WT's can also be installed on rougher sea floors, but they can only handle water depths of up to 28m [5] (see Figure 1.3). Jackets in contrast can be built in waters with a depth of up to 70m [5] (see Figure 1.1). However, they are more complex in manufacturing than e.g. monopiles. To open up new areas for offshore wind parks, governments and companies are working on floating solutions. They could be installed in deeper waters of which a vast amount is available and till now unused. There are three main types of floating WT's: spars, semi-submersibles and tension leg platforms (TLP) (see Figure 1.4, 1.5 and 1.6).

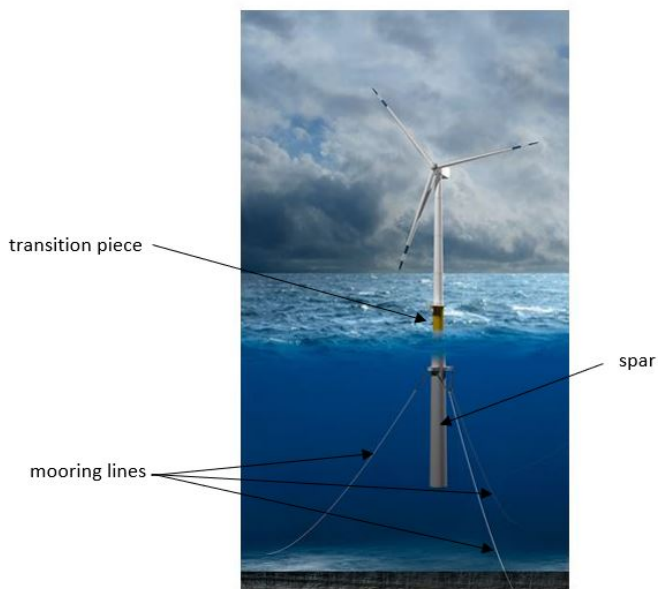


Figure 1.4: Spar OWT [6]

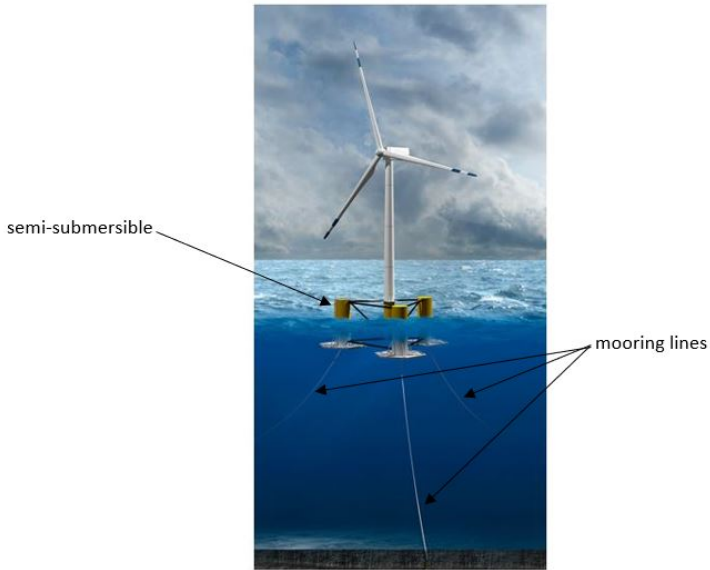


Figure 1.5: Semi-submersible OWT [6]

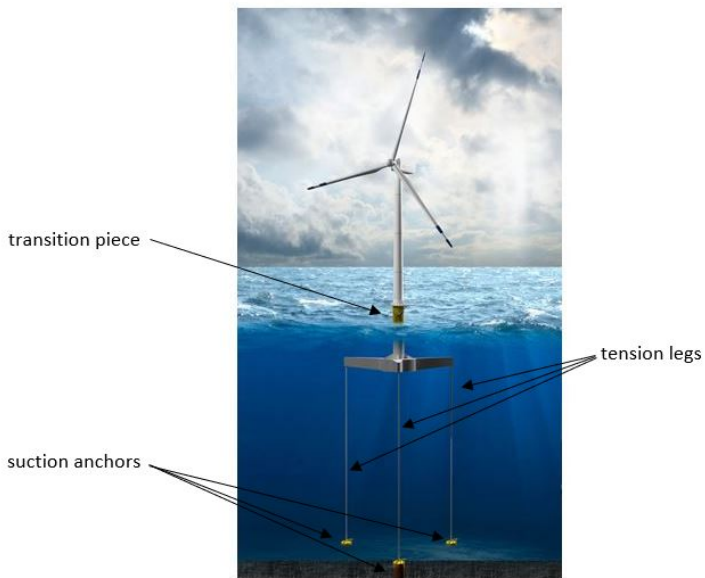


Figure 1.6: TLP OWT [6]

Only spars and semi-submersibles have been built so far. In regards to semi-submersibles, only two projects have been carried out in full scale [4]. One was the WindFloat in the Atlantic ocean 5km off the coast north of Porto, Portugal. The other project was the Fukushima floating offshore wind farm. So over all, two 2MW and one 7MW semi-submersible WTs have been installed till now. In the course of the Fukushima project, also one spar WT has been installed. Besides in Japan, an offshore spar wind farm consisting of five WTs has been built 29km off Peterhead in Scotland. The Hywind park.

1.2 Motivation

The main motivation to design a floating dock for spar WTs arose from the Hywind project which was completed in 2017. The next three subsections give an overview about the project, what has been done and what turned out to be a challenge. The floating dock concept aims to overcome some of these challenges.

1.2.1 Norway Hywind Demo

The first Hywind turbine was built by Equinor at the Norwegian west coast in 2009 (see Figure 1.7). It is a demo version and was supposed to proof the concept of a floating spar wind turbine. It weighs 5300tons and has a draught of 100m at a water depth of 220m. The spar has a diameter of 8.3m and is moored to the drag embedded anchors by wires and chains. The hub height of the 2.3MW turbine amounts 65m and the rotor diameter is 85m. [8] [9] Since the demo version is installed in the same way as the Hywind park turbines, the installation procedure of Hywind turbines is discussed in detail in the next section.

From 2010 till 2013 the demo version produced 8.3GWh per year and thus supplied electricity to 1629 households annually. The Hywind turbine produced better than expected. So that a Hywind farm was developed on basis of the information collected by the demo version. [8]

However, the demo version has not been decommissioned yet and is still operating.



Figure 1.7: Norway Hywind Demo [7]

1.2.2 Scotland Hywind Park

The Hywind Park consists of five Hywind turbines installed 29km off Peterhead in Scotland. It was permissioned by the

Scottish government in 2015. At that time, the Norwegian government did not make an installation in Norway possible. [10]

The design of the five Hywind turbines bases on the demo version, but they are up-scaled from 2.3MW to 6MW. So that one offshore wind turbine (OWT) weighs 11200tons with a maximum spar diameter of 14.4m and a rotor diameter of 154m. The hub height is 98m and the draught on site at a water depth of approximately 105m amounts 78m. The anchors are unlike the demo version designed as suction anchors. They are 16m tall, approximately 111tons heavy and have a diameter of 5m. The anchors (Global) were constructed in Scotland. While the spars (Navantia) and towers (Navacel) were built in Spain. The turbines (Siemens) in turn were produced in Denmark. [10]

All components were then transported to Stord on the west coast of Norway where they were stored and sampled in 2017. The final pieces to arrive and stored were the substructures. They were wet-towed in a horizontal position and then up-ended by filling 8000tons of seawater in the ballast tanks. After that, the spars were filled with around 5500tons of iron ore while pumping out again approximately 5000tons of seawater to maintain the draft. The turbines were completely assembled onshore and then mated with the spar using the Saipem 7000 floating crane [11]. The OWTs were stored one after another on three barges while the preparations for transit were made. [12] On mid-July 2017, the first wind turbine was ready to be towed to Scotland (see Figure 1.8).



Figure 1.8: Transportation of Hywind turbines [13]

It was towed by four anchor handling tug supply vessels within four days from Stord to the site in Scotland. Concerning the towing operation, an analysis was made beforehand in Orcaflex, a simulation was done by Marintek, a survey of the fjord was conducted and in regards to vortex induced motions (VIM), a towing test was performed by Sintef in Trondheim [12]. The last Hywind turbine arrived in Scotland without complications in mid-August [11]. After their arrival, the spars were connected with mooring chains to the suction anchors which had already been installed on site. Each spar were connected to three mooring chains and anchors. The chains are made of steel and each chain link has a thickness of 15cm, a length of 0.5m and a weight of 450kg [14]. In addition, weights of

60tons were attached to the midpoint of each anchor line to provide additional tension. All five OWTs were then integrated in a grid connected to an export cable taking the produced electricity to shore (see Figure 1.9). After final testing, the Hywind Park was handed over from installation to operation in October 2017. [10]

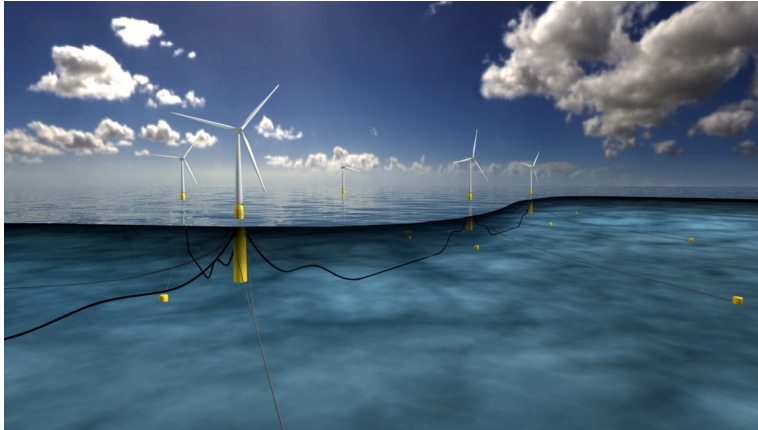


Figure 1.9: Hywind Scotland - Illustration Equinor [10]

The next three month, the park generated at an average of 65% and performed hereby better than expected. The cost per MW were cut by 60% from the Hywind demo to the Hywind park. In addition the Hywind turbines had encountered hurricane Ophelia in October and in early December Storm Caroline with maximum wave heights of 8.2m. During that storm, the park was forced to shut down temporarily for safety reasons, but the turbines automatically resumed operation afterwards. [15] A technology-qualification-program collects all information. The data is evaluated and may contribute to the development of new Hywind projects. [10]

1.2.3 Resulting Challenges

In the course of the Hywind Park project, several challenges, expected and unexpected ones, were faced. The main challenges according to Leif Delp (Project Director, Equinor) turned out to be the tight execution, the interface between contractors, the conversion of new technology and the heavy lift operations [16]. There have been 15 main contractors with even more subcontractors for the Hywind Park project. Six of them are Norwegian companies, the remaining are situated in various countries around Europe.[14] The coordination and timeliness of each company influenced the execution timetable for the whole project. Time scheduling was also made difficult by the fact that no floating spar OWT park has been built and installed before. The basis of the project was the experiences gained from the Hywind Demo, the installation of spar platforms and bottom-fixed OWTs.

[16] Also the heavy lift operations presented a major challenge. Lifting the fully sampled turbine onto the floating substructure was only possible with a specific crane vessel, at a site of high depth due to the deep draft of the spar and only during very calm weather conditions so that the relative motions between spar top and tower bottom could be kept under control (see Figure 1.10). [16]



Figure 1.10: Lift operation Hywind Scotland [16]

Despite those challenges, Equinor plans to further develop the Hywind concept. The next step may be the development of a complete offshore Hywind farm with 40 till 60 wind turbines, similar to bottom fixed wind farms [14]. Also new areas could open up for such a project. According to Irene Rummelhoff (Executive Vice President for New Energy Solutions, Equinor), there is great potential for floating offshore wind on the west coast of North America and in Asia, in particular Japan where the water is too deep for bottom fixed OWTs in most of its areas. One goal for the next Hywind park is certainly to reduce the costs and improve the competitiveness of the Hywind turbines with respect to the bottom fixed ones. [16] There are several approaches to achieve that. One is to standardize more operations in the construction and installation process. Standard turbines, standard installation vessels and so forth could be used. Moreover common anchor points reducing the number of anchors per unit could be established and the substructure could be optimized with respect to material use and production friendliness. [8] Another approach aiming mainly for a reduction of transportation costs as well as reduction of costs for heavy lift vessels (HLV) is the floating dock concept presented in the next section.

1.3 Main Concept

The main concept comprises a floating dock that is moored on site with chains to the sea bed. The floating dock is shaped as a vertical tube giving space to install the Hywind turbines in its center and storing the components dryly on the top of its sides. It gives also space for cranes, living accommodation, offices and a landing platform (see Figure 1.11).

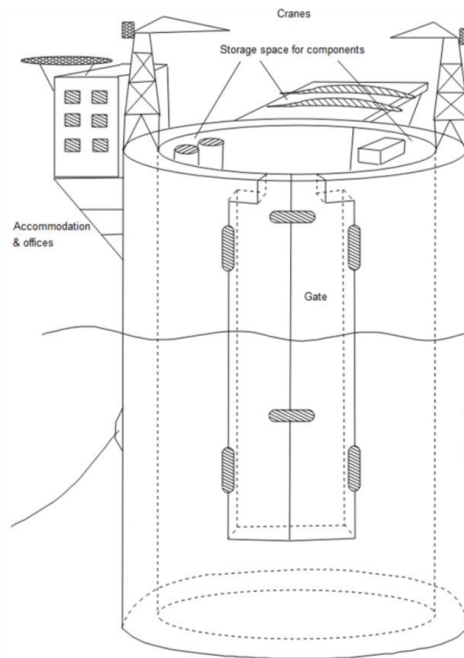


Figure 1.11: Main concept [17]

The basic idea of this concept is that the turbines are completed in the floating dock close to the site and not at a shipyard from where they have to be towed to the site like in course of the Hywind project. As already mentioned in Section 1.2.3 'Resulting Challenges', the towing operation was one of the most elaborate aspects in that project. Analyses, simulations, a model test and a survey of the fjord had to be conducted to ensure that the towing operation would be successful. Furthermore the shipyard chosen to complete the wind turbines had to have a certain water depth and the world's second largest crane vessel was needed to lift the completed wind turbine onto the spar. In case of the floating dock concept, the components could be installed onto the spar using another installation method.




























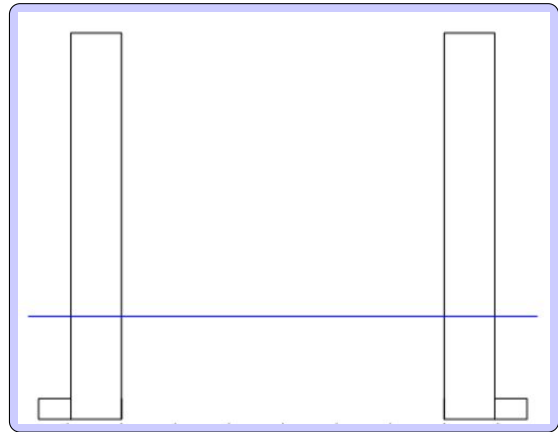
Components and weights	Installation method	Number of lifts					
		1	2	3	4	5	6
2 tower sections:  173.75 ton each	1						
	Lift weight	173.75	173.75	300.5	16.5	16.5	16.5
nacelle:  240 ton	2						
	Lift weight	347.5	300.5	16.5	16.5	16.5	
hub:  110 ton	3						
	Lift weight	173.75	173.75	240	110		
3 blades:  16.5 ton each	4						
	Lift weight	173.75	173.75	333.5	16.5		
	5						
	Lift weight	347.5	333.5	16.5			
	6						
	Lift weight	697.5					

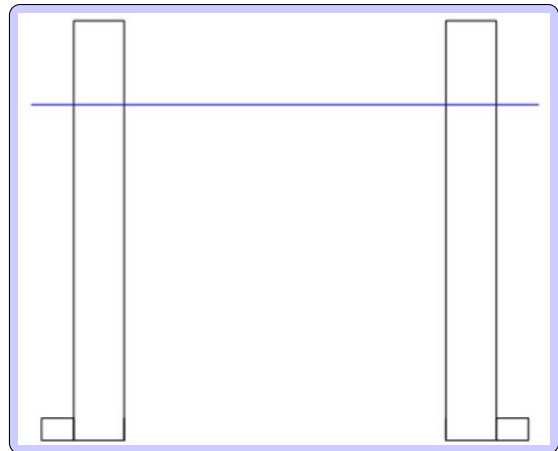
Figure 1.12: Different installation methods of turbine components [5]

Choosing for example installation method 1 or 2 from Figure 1.12 above, the maximum lift weight amounts only around 620tons (weight of the tower). A crane with less capacity than the Saipem 7000 can handle this. The cylindrical shape of the dock has also the advantage that the turbine is shielded to a certain extent from wind and waves. In addition, the floating dock can be towed to every desired site. Its mooring lines are cleared, the ballast water is reduced so that the dock has only a limited draft (transit mode) and then it can be towed by tug vessels to another site where it is ballasted and fixed with mooring lines again (operational mode).

Dock is towed to the site



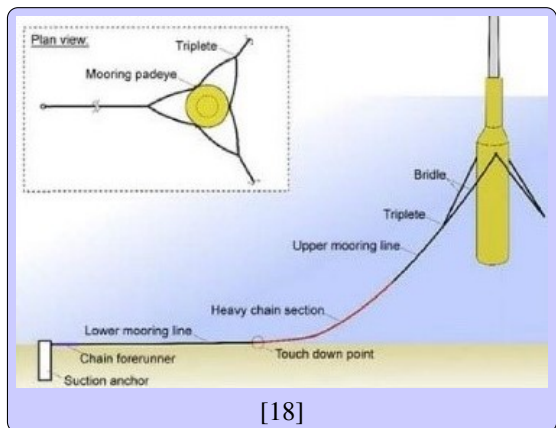
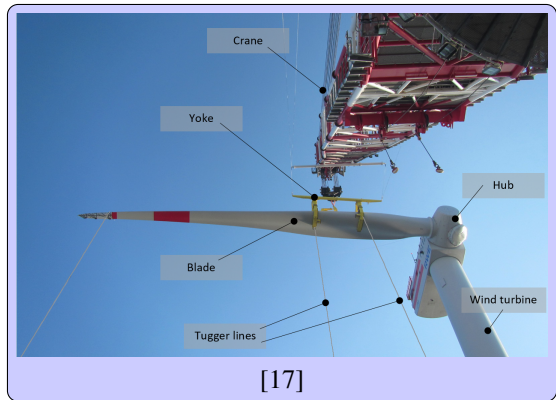
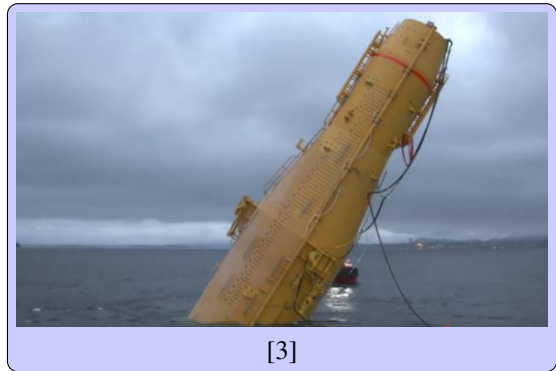
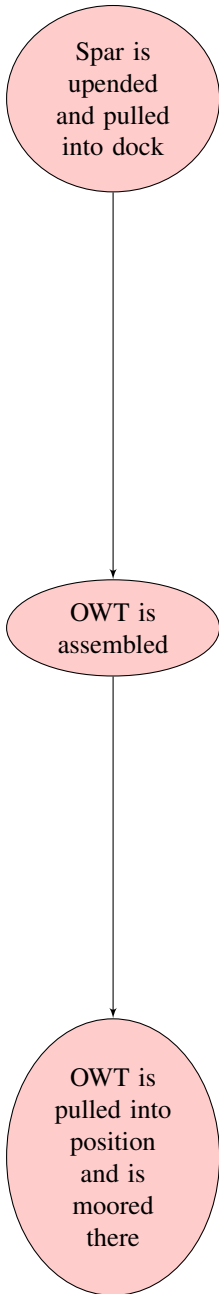
Dock is ballasted and moored



Spar is towed horizontally to dock



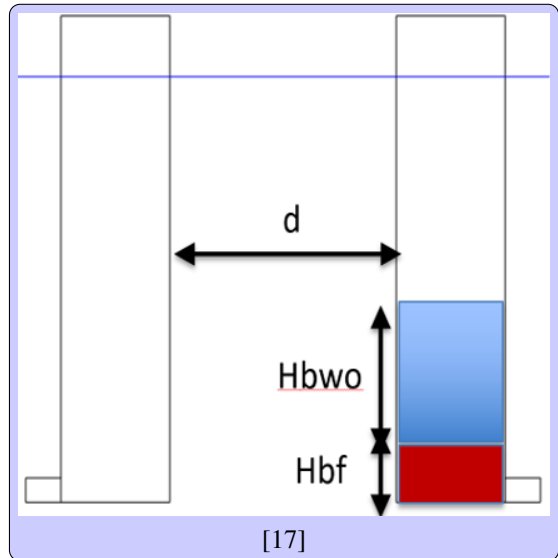
[4]



no more
OWTs to
install?

Dock is
unmoored
and
unballasted

Dock is
towed to
shipyard



Chapter 2

Theory

In the course of the thesis, several theories and terms are used. The following section provides an overview of the essential ones. The effects and approaches are briefly explained and reasons for their importance are given.

2.1 Sloshing Effects

Sloshing effects occur when a liquid inside another object interacts with the movement of the container. This is the case for example for spacecraft tanks, trucks transporting liquids or swimming pools on cruise ships. With regards to the project, sloshing means that the free water surface within the dock elevates as a consequence of the dock motion. This elevation can cause high pitch and heave motions for the spar inside the dock. The motions can become critical if sloshing resonance occurs.

The most important resonance is called piston-mode oscillation. Piston means here that the water moves in nearly one dimension as a rigid body in the floating dock [19]. Those movements are induced by the heave motion of the dock which acts as excitation. The piston-mode resonance frequency occurs when there are relatively large dock motions in heave [19]. Those arise when waves with large significant wave heights impinge on the dock. The resonance also highly depends on the water-depth-to-dock-diameter ratio [19]. The higher the water depth in the floating dock, the larger the motion of the free surface in the dock for given heave dock motions.

At the current state of the project, sloshing effects were taken into account by considering linear potential flow theory and solving the spectral problem shown in Figure 2.1.

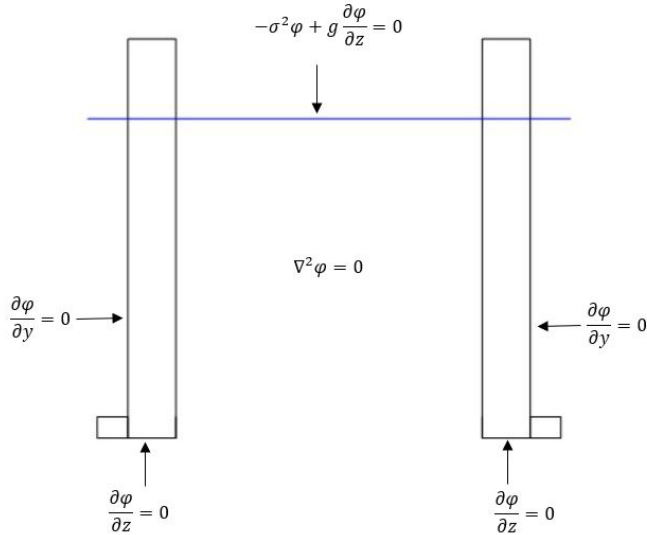


Figure 2.1: Spectral problem

The main difference to internal sloshing in tanks or swimming pools is that global conservation is not posed. The water flows in and out through the bottom opening of the dock. In regards to the calculation made, one should also mention, that the spar inside the dock was not included. However, this simplification was acceptable since the spar provides only insignificant damping and radiation force. The critical aspect was the exclusion of viscous effects. The main damping comes from the shed vortices at the dock inlet (see Figure 2.2 on the next page). They arise due to flow separation at sharp corners and are classified as viscous effects. Excluding them resulted in a significant impact on the RAO results. That is why additional empirical linearized damping was specified in the computing program. The major proportion was set near the sloshing period, where the added mass and radiation damping jump significantly in reality.

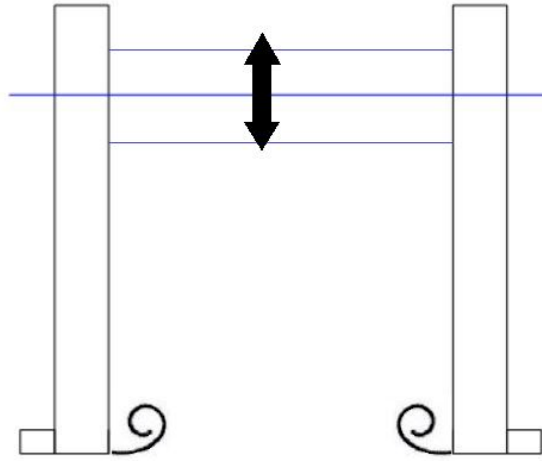


Figure 2.2: Viscous damping

When estimating the sloshing period, the specified damping did not affect the result. In this way, the sloshing resonance was determined to occur at around 7s and piston resonance at around 20s. But one has to keep in mind that in reality, viscous effects provide additional damping and may affect the calculation in a way that sloshing induced spar motions decrease.

2.2 Coupling Effects

When determining the motion of the spar inside the dock, one must also take the motion of the dock itself into account and the other way around. Both bodies are coupled since they are connected through mooring lines. Coupling effects are respected by using the coupled equation of motion. This equation is derived from Newton's second law.

$$M\ddot{x} = F \quad (2.1)$$

The mass of a body times its acceleration is equal to the net force applied. Taking into account that the net force is the excitation force minus added mass, damping and hydrostatic restoring gives

$$M\ddot{x} = F_{exc} - A\ddot{x} - B\dot{x} - Cx \quad (2.2)$$

This can be reformulated as

$$(M + A)\ddot{x} + B\dot{x} + Cx = F_{exc} \quad (2.3)$$

Formula 2.3 describes the basic equation of motion, where M is the mass, A the added mass coefficient, B the damping coefficient and C the stiffness coefficient of the body. For an uncoupled single-body system, the coefficients are 6x6 matrices. One row and column for every degree of freedom (DOF).

$$A = \begin{bmatrix} a_{11} & \dots & a_{16} \\ \vdots & \ddots & \vdots \\ a_{61} & \dots & a_{66} \end{bmatrix} \quad (2.4)$$

$$B = \begin{bmatrix} b_{11} & \dots & b_{16} \\ \vdots & \ddots & \vdots \\ b_{61} & \dots & b_{66} \end{bmatrix} \quad (2.5)$$

$$C = \begin{bmatrix} c_{11} & \dots & c_{16} \\ \vdots & \ddots & \vdots \\ c_{61} & \dots & c_{66} \end{bmatrix} \quad (2.6)$$

Whereby, the first index describes the resulting force, while the second the forced motion. So e.g. a_{12} describes the added mass in surge motion caused by forced sway motion. To describe now a coupled system of two bodies, the coefficients' matrices have to be modified to 12x12 matrices:

$$A = \begin{bmatrix} A_{11} & A_{12} \\ A_{21} & A_{22} \end{bmatrix} \quad (2.7)$$

$$B = \begin{bmatrix} B_{11} & B_{12} \\ B_{21} & B_{22} \end{bmatrix} \quad (2.8)$$

$$C = \begin{bmatrix} C_{11} & C_{12} \\ C_{21} & C_{22} \end{bmatrix} \quad (2.9)$$

The indices indicate hereby by which body a force is caused and on which body the force acts. So for example A_{12} is the added mass matrix in regards to added mass forces caused by body 2 (the OWT) acting on body 1 (the dock). A_{11} is consequently the uncoupled 6x6 added mass matrix of the dock, while A_{22} is the uncoupled 6x6 added mass matrix of the OWT.

When all coefficient are established, the sloshing forces are added to the excitation force F_{exc} and the motion of the spar or dock can be determined. This theory applies of course not only for the spar but also for other bodies coupled to the dock (see also Section 3.3.3 'Input to SIMA').

2.3 Response Amplitude Operator

In this thesis, the motion of the numerical model should be brought into line with the motion of the model in the model tests. Since the model tests are conducted with a scale factor of 100, only scaled or non-dimensional values are comparable. Assessing the non-dimensional Response Amplitude Operators (RAO) ensures a reliable and easy comparison between the down-scaled model tests and the numerical full scale simulations.

RAOs are effectively transfer functions used to determine the effect that a sea state has upon the motion of a floating system. They can only be defined when the system's motions are linear [20]. This assumption is met when the system is under regular wave conditions. Then the RAO can easily be calculated by dividing the response amplitude by the excitation amplitude. This means in the current case dividing the dock motion by the wave amplitude (see also Figure 2.3).

$$(M + A)\ddot{x} + B\dot{x} + Cx = F \quad (2.10)$$

with $x = a \cdot e^{i\omega t}$

$$F = F_0 \cdot \zeta_a \cdot e^{i\omega t}$$

$$(M + A)(-\omega^2 \cdot a e^{i\omega t}) + B(i\omega \cdot a e^{i\omega t}) + C(a e^{i\omega t}) = F_0 \cdot \zeta_a e^{i\omega t} \quad (2.11)$$

$$\text{RAO} = \frac{a}{\zeta_a} = \frac{F_0}{-\omega^2(M + A) + i\omega B + C} \quad (2.12)$$

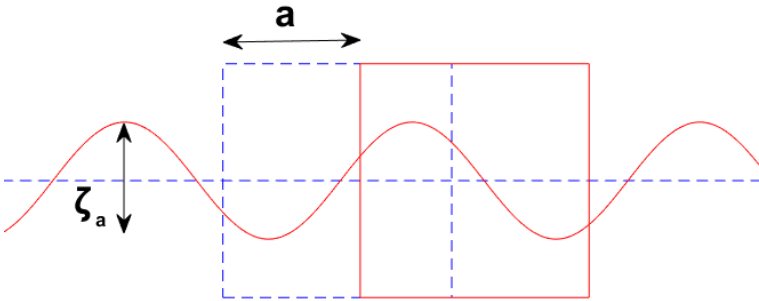


Figure 2.3: RAO variables in surge

Chapter 3

Numerical Modelling

In this chapter, two numerical approaches to establish a calibrated hydrodynamic model of the floating dock are presented.

To begin with, the work done prior to this thesis is briefly summarized. The model tests are discussed more closely since ensuing modifications are conducted on their basis. After that, the two numerical approaches are set out. For the first approach, the computer program WAMIT is introduced and reasons are given why it was chosen to conduct the hydrodynamic analysis of the dock. The model in WAMIT is then presented and calibrations done are set out. The subsequent subsections discuss the export of the model from WAMIT to the computer program SIMA. Here it is also reasoned why this program was chosen and how and why modifications were done. The section presenting the second approach is subdivided the same way but on basis of the information given for the first approach.

3.1 Previous Work

After Equinor proposed the idea of a floating dock for spar wind turbines, the Department of Marine Technology at the Norwegian University of Science and Technology (NTNU) started to work out and validate the concept. First the conceptual design was assessed by examining the stability of the transit and operational mode in regards to dynamic performance in waves.

After the validation of the conceptual design, the dimensions were optimized by 11 design parameters which can be found in Table 3.1 with current values (see also Figure 3.1). Those optimizations were performed in Matlab precluding dynamic motions conducted by Zhiyu Jiang and his supervisor Zhen Gao.

Outer diameter (m)	D_o	80.3
Inner diameter (m)	D_i	60
Height of fixed ballast (m)	H_{bf}	12.5
Steel weight (tons)	M_{st}	$1.0566 \cdot 10^4$
<i>Operational condition</i>		
Draft (m)	T_o	65
Freeboard (m)	F_o	20
Height of ballast water (m)	H_{bwo}	48.54
Outward extension of bilge box (m)	B_{osk}	6.0
Inward extension of bilge box (m)	B_{isk}	0.0
Displacement (tons)	Δ_o	$1.9687 \cdot 10^5$
Payload with 5 wind turbines (tons)	W_o	$1.55 \cdot 10^4$
Vertical center of gravity (m)	KG_o	23.06
<i>Transit condition</i>		
Draft in transit (m)	T_t	20
Freeboard (m)	F_t	65
Height of ballast water (m)	H_{bwt}	0.0
Displacement (tons)	Δ_t	$9.3677 \cdot 10^4$
Payload with 5 wind turbines (tons)	W_t	6000
Vertical center of gravity (m)	KG_t	18.52

Table 3.1: Design variables with latest values

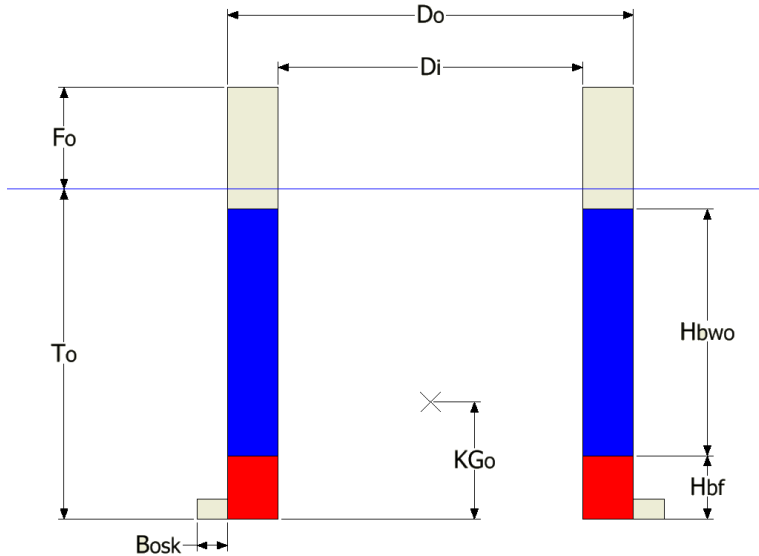


Figure 3.1: Design variables in operational condition

The optimizations were done with respect to performance and cost of the dock. This means that the steel weight was set as the objective function, while the static heeling angle was set as a constraint. There were also other constraints set in regards to the design variable, limiting the possible number of variations. Those were for example a maximum draft in transit of 20m due to the depth of the Suez Canal or a minimum draft in operation of 120m due to the size of the spar (see Appendix A). Furthermore there were several constraints concerning the safety and stability of the dock, like e.g. a minimum GM of 1m in operation and transit (see Appendix A). The resulting dimensions are the basis for further analyses, but are also still under reserve.

To the current point of time, hydrodynamic load and motion analyses are performed. The hydrodynamic analysis determines in frequency domain the added mass, the wave excitation force and the radiation damping of the spar and the dock. Thereby, only linear damping is considered while stiffness is not further specified. In the time-domain motion analysis, the equations of motion are solved considering both the hydrodynamic coupling and the mechanical coupling between the spar and dock.

In addition to those analyses, a serie of model tests was executed by Maël Moreau and his supervisor Trygve Kristiansen in towing tank III of Sintef Ocean, Trondheim (see Figure 3.2).

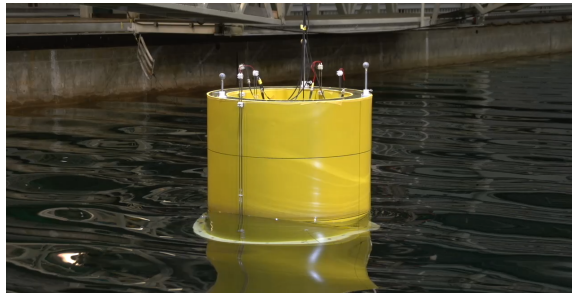


Figure 3.2: Model test

The tests base on the results of the optimization and were performed with a simplified model of the dock scaled down by a factor of 100. The model was equipped with eight wave gauges attached to the inner and outer walls of the dock. It was fixed to the towing carriage by a rope/spring system allowing it to move freely in all six directions of freedom. No OWT model was moored inside the dock. The tests were performed with two different drafts, 50 and 80m in full scale and two different sizes of bilge tanks. Since the tests were conducted in an earlier stage of the optimization, the dimensions differ partly from the present ones. Table 3.2 shows the design variables in the setting with the minimum differences to the current readings.

		<i>Dimension model test in model scale</i>	<i>Dimension model test in full scale</i>	<i>Difference to present dimensions in full scale</i>
Outer diameter (m)	D_o	0.8	80	0.3
Inner diameter (m)	D_i	0.6	60	0
<i>Operational condition</i>				
Draft (m)	T_o	0.8	80	15
Freeboard (m)	F_o	0.25	25	5
Outward extension of bilge box (m)	B_{osk}	0.06	6	0
Inward extension of bilge box (m)	B_{isk}	0.0	0	0
Displacement (tons)	Δ_t	0.1861	$1.8612 \cdot 10^5$	$1.0750 \cdot 10^4$
Vertical center of gravity (m)	KG_o	0.236	23.6	0.54

Table 3.2: Design variables in model test (Set 2)

However, all test settings were tested under the same regular wave conditions varying between 5 and 25s full scale with a constant wave steepness of 1/60. Three sets of wave periods were applied. Set 1 with a wide range of periods, Set 2 with periods close to the sloshing period of the dock and Set 3 with periods close to the piston period of the dock (see Appendix B).

Up to this point of time, the model test results seem to confirm the numerical results to a certain extent. However, the eigenperiods found by the model test are somewhat lower than the ones found numerically in WAMIT. There are several possible causes for that, e.g. non-linear effects or coupling between sloshing and natural period.

Taking this as a starting point for the thesis, one goal is naturally the adjustment or regeneration of the numerical model to the physical model of the tests. In a second step, after adjusting the model with regards to regular waves, the behaviour of the dock in irregular waves can be examined and assessed.

3.2 First Approach

3.2.1 Introduction to WAMIT model

WAMIT is a program that analyzes the hydrodynamic response of floating structures in waves. The structure, in this case the floating dock, is represented by small quadrilateral panels on which the velocity potential is assumed constant. Based on the linear potential theory, solutions for the diffraction and radiation problems are carried out simultaneously.

To run a basic application in WAMIT, three different input files are required.

- The geometric data file (.gdf) specifies the geometry of the body. Its wetted surfaces are divided into a number of four-sided panels. Each panel is discretised by the Cartesian coordinates x,y,z of its four vertices. In addition to that, the body length scale, gravity, symmetry indices and the total number of panels is specified in the geometric data file. [21] The total number of panels depends hereby on the model type. The user can choose between a high and a low order panel model.

- The potential control file (.pot) is used to input various parameters like the dimensional water depth, the wave periods and the wave direction. Moreover, it defines the position of the bodies in the global coordinate system, their corresponding geometric data file and their degree of freedoms. [21]

- The force control file (.frc) is used to input various parameters to the FORCE sub-program. There are two alternative forms. In the first one, the input of the body inertia matrix is simplified, and it is assumed that the body is freely floating. In the second form, it is possible to specify separately three independent external force matrices including the mass matrix of the body, an external damping matrix, and an external stiffness matrix. This permits the analysis of bodies, that are not freely floating in waves, with arbitrary linear external forces and moments and it also permits the specification of the complete body mass matrix instead of the simpler radii of gyration. [21]

There are other input files that can be prepared in addition to those three, for example the configuration file (.cfg) and the filenames list file (.wam). Both are optional configuration files that may be used to specify various parameters and options. In the configuration file for example, the maximum number of iteration can be set. And the filenames list file indicates among other things the input files.

In case of the first approach, the five files mentioned above are generated by a set of Matlab files compiled by Maël Moreau. In those files, all necessary information are stored like e.g. the dimensions of the model and the environmental conditions. Also the body is discretised and meshed in Matlab (see Figure 3.3).

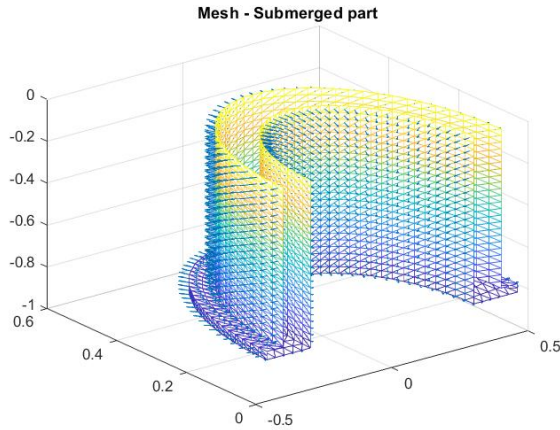


Figure 3.3: Dock meshing

Besides that, the inertia, damping and restoring terms due to mooring are calculated. Based on the information and calculation of Matlab, the input files for WAMIT are created.

The reason why the calibration process is done in WAMIT is that the program solves not only the RAOs of the dock but also the wave elevation inside the dock. During the model test the wave elevation inside the dock was measured at eight different positions. Those data sets need to be compared to the numerical ones. Another advantage of WAMIT is that its calculations are based on non-dimensional values. In this way it becomes easier to transfer between model and full scale.

3.2.2 Calibration of WAMIT model

A number of changes are made to the WAMIT model. First of all, the provided Matlab files are modified. The design variables and environmental parameter are up-scaled by means of the Froude scaling laws.

<i>Physical Parameter</i>	<i>Unit</i>	<i>Factor</i>	<i>Factor Model Tests</i>
Length	[m]	λ	100
Structural mass	[kg]	$\lambda^3 \cdot \rho_F / \rho_M$	$1 \cdot 10^6$
Force	[N]	$\lambda^3 \cdot \rho_F / \rho_M$	$1 \cdot 10^6$
Moment	[Nm]	$\lambda^4 \cdot \rho_F / \rho_M$	$1 \cdot 10^8$
Acceleration	[m/s ²]	$a_F = a_M$	1
Time	[s]	$\sqrt{\lambda}$	10
Pressure	[Pa=N/m ²]	$\lambda \cdot \rho_F / \rho_M$	100

Table 3.3: Froude scaling table [22]

Then the mass and stiffness properties are checked and modified.

The mass is the product of displacement times water density.

$$M = \nabla \cdot \rho_W = 1.8158 \cdot 10^8 kg \quad (3.1)$$

The moments of inertia are separately calculated for the structure, the skirt and the ballast (see also Figure 3.4). They are then added using the parallel axis theorem.

- Structure

$$I_{4St} = I_{5St} = \frac{r_2}{r_2 + r_1} \cdot \frac{M_{St}}{12} \cdot (6 \cdot r_2^2 + H^2) + \frac{r_1}{r_2 + r_1} \cdot \frac{M_{St}}{12} \cdot (6 \cdot r_1^2 + H^2) \quad (3.2)$$

$$I_{6St} = \frac{r_2}{r_2 + r_1} \cdot M_{St} \cdot r_2^2 + \frac{r_1}{r_2 + r_1} \cdot M_{St} \cdot r_1^2 \quad (3.3)$$

- Skirt

$$I_{4,sk} = I_{5,sk} = \frac{M_{sk}}{12} \cdot (3 \cdot ((B_{sk} + r_2)^2 + r_1^2) + H_{sk}^2) \quad (3.4)$$

$$I_{6,sk} = 0.5 \cdot ((B_{sk} + r_2)^2 + r_1^2) \cdot M_{sk} \quad (3.5)$$

- Ballast

$$I_{4,b} = I_{5,b} = \frac{M_b}{12} \cdot (3 \cdot (r_2^2 + r_1^2) + H_b^2) \quad (3.6)$$

$$I_{6,b} = 0.5 \cdot (r_2^2 + r_1^2) \cdot M_b \quad (3.7)$$

- Total

$$\begin{aligned}
 I_4 = I_5 = & I_{5st} + \underbrace{0.5 \cdot M_{st} \cdot (d - f - H_{sk}^2)}_{\text{Parallel axis contribution of structure}} \\
 & + I_{5sk} + \underbrace{M_{sk} \cdot (d - z_{sk})^2}_{\text{Parallel axis contribution of skirt}} \\
 & + I_{5b} + \underbrace{M_b \cdot (d - z_b)^2}_{\text{Parallel axis contribution of ballast}}
 \end{aligned} \quad (3.8)$$

$$I_6 = I_{6st} + I_{6sk} + I_{6b} \quad (3.9)$$

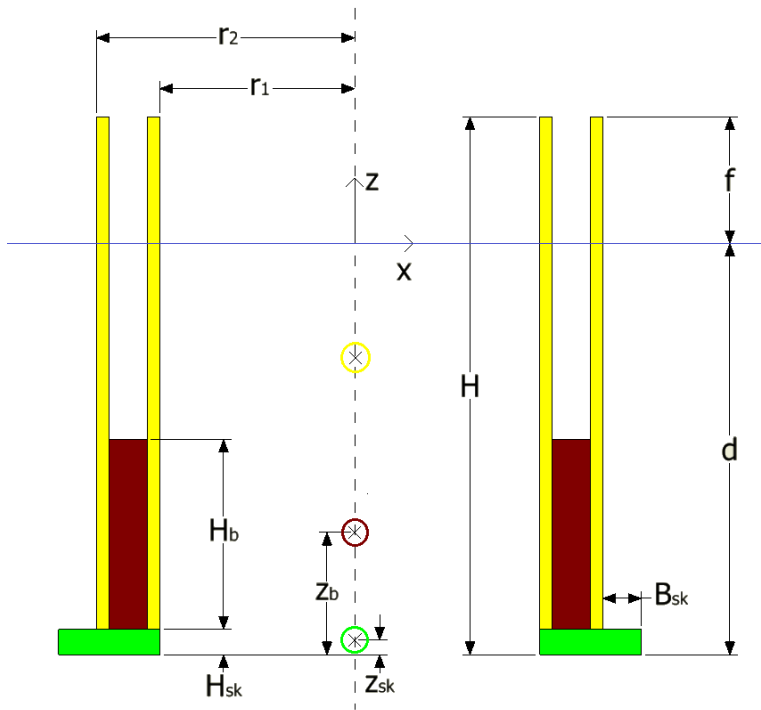


Figure 3.4: Moment of inertia - Variables

So that the mass matrix is updated to

$$\begin{bmatrix} M & 0 & 0 & 0 & 0 & 0 \\ 0 & M & 0 & 0 & 0 & 0 \\ 0 & 0 & M & 0 & 0 & 0 \\ 0 & 0 & 0 & I_4 & 0 & 0 \\ 0 & 0 & 0 & 0 & I_5 & 0 \\ 0 & 0 & 0 & 0 & 0 & I_6 \end{bmatrix}$$

$$\begin{bmatrix} 1.82 \cdot 10^8 & 0 & 0 & 0 & 0 & 0 \\ 0 & 1.82 \cdot 10^8 & 0 & 0 & 0 & 0 \\ 0 & 0 & 1.82 \cdot 10^8 & 0 & 0 & 0 \\ 0 & 0 & 0 & 7.04 \cdot 10^{11} & 0 & 0 \\ 0 & 0 & 0 & 0 & 7.04 \cdot 10^{11} & 0 \\ 0 & 0 & 0 & 0 & 0 & 2.30 \cdot 10^{11} \end{bmatrix}$$

The stiffness matrix of the mooring system is determined based on the pretension and the stiffness of the lines. In the model tests, they are attached to the dock as sketched in Figure 3.5 and 3.6 on the next page.

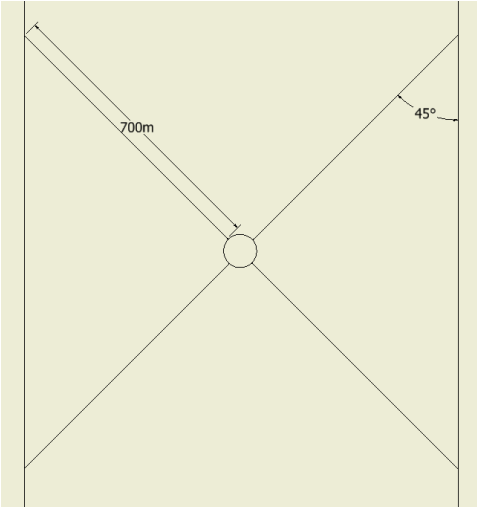


Figure 3.5: Mooring system in top view

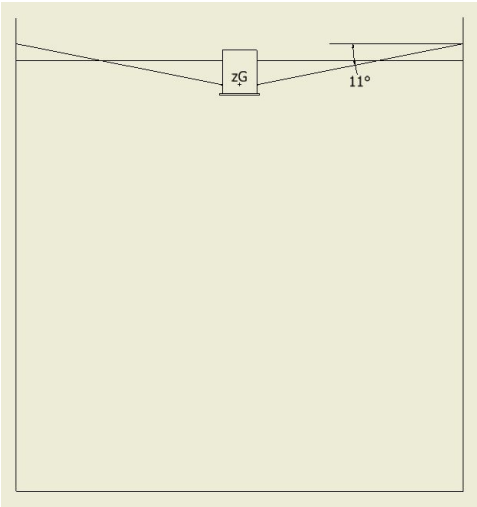


Figure 3.6: Mooring system in side view

With a length L , a pretension F_{pret} and a stiffness k_M per line, the stiffness matrix is established by

$$k_1 = k_2 = 2 \cdot k_M \cdot \cos(11^\circ) \cdot \cos(45^\circ) \quad (3.10)$$

$$k_3 = 4 \cdot k_M \cdot \sin(11^\circ) \quad (3.11)$$

$$k_4 = k_5 = r_2 \cdot F_{pret} \cdot 2 \cdot \cos(11^\circ) \cdot \cos(45^\circ) \quad (3.12)$$

$$k_6 = (k_M \cdot \Delta L + F_{pret}) \cdot \sin(\psi) \cdot L \cdot \frac{4}{\psi} \quad (3.13)$$

r_2 = outer diameter of dock

ψ = motion in yaw [deg]

$$\begin{bmatrix} k_1 & 0 & 0 & 0 & 0 & 0 \\ 0 & k_2 & 0 & 0 & 0 & 0 \\ 0 & 0 & k_3 & 0 & 0 & 0 \\ 0 & 0 & 0 & k_4 & 0 & 0 \\ 0 & 0 & 0 & 0 & k_5 & 0 \\ 0 & 0 & 0 & 0 & 0 & k_6 \end{bmatrix}$$

A length of 700m, a pretension of $6.5 \cdot 10^7$ N and a stiffness of $1.2 \cdot 10^6$ N/m per line results thus into following stiffness matrix for the mooring system.

$$\begin{bmatrix} 1.66 \cdot 10^6 & 0 & 0 & 0 & 0 & 0 \\ 0 & 1.66 \cdot 10^6 & 0 & 0 & 0 & 0 \\ 0 & 0 & 9.38 \cdot 10^5 & 0 & 0 & 0 \\ 0 & 0 & 0 & 3.88 \cdot 10^9 & 0 & 0 \\ 0 & 0 & 0 & 0 & 3.88 \cdot 10^9 & 0 \\ 0 & 0 & 0 & 0 & 0 & 3.18 \cdot 10^9 \end{bmatrix}$$

Having modified those two matrices, the model is run in WAMIT for wave periods between 5 and 25s with different wave headings.

3.2.3 Input to SIMA

The results of the WAMIT simulations are stored in an output file which can be imported to SIMA. SIMA supports WAMIT version 7.06. The tasks in WAMIT have the same basic components as the physical engines in SIMO, one of the solvers in SIMA.

- location
- environment
- body
- calculation parameters

In the location component, water density, gravitational acceleration and water depth are set. Wave headings and periods are set under environments. The body is specified by the geometric data file. Also body origin coordinates, coordinates of the center of gravity (CoG), control surfaces, external mass, damping and stiffness matrices are included in this section. However, it is important to note that the stiffness matrix from the mooring system of the dock is not taken over from WAMIT. The calculation parameters are separated into two tabs; one for the static calculation and one for the dynamic one. Here the maximum period, the tolerance in position and direction, the time step and the maximum number of steps are defined.

The main reason why the model is imported to SIMA is that it carries out simulations in time domain rather than frequency domain as WAMIT does. Environmental conditions can also be varied easily. So that real-life scenarios can be simulated and assessed. Furthermore slender elements can be added to account for viscous effects.

3.2.4 Modification in SIMA

After the WAMIT output file is imported to SIMA, several modifications are done in order to bring the numerical model closer to the physical one.

First of all, the stiffness matrix of the mooring system is added to the stiffness matrix of the dock. When importing the WAMIT model to SIMA, all information about the mooring system drop away so that the mooring system has to be modelled again. There are several opportunities to do that. A catenary system or fixed force elongations providing the same stiffness as the lines in the model test can be created. But the most straightforward method is to add the stiffness matrix of the mooring system, which was already calculated for the WAMIT model, to the stiffness matrix of the dock.

In a second step, slender elements are created to account for viscous effects. One slender element for the dock, one for the skirt and eight forming a octagon for the bottom edge of the skirt (see Figure 3.7).

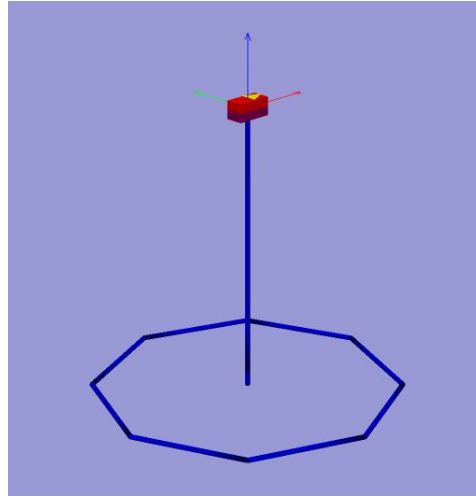


Figure 3.7: Formation of slender elements

The drag coefficient of each slender element is calculated with regards to DNV-RP-C205 section '6.7.2 Effect of Keulegan Carpenter number'.

$$C_D = C_{DS}(\Delta) \cdot \psi(K_C) \quad (3.14)$$

with

$$C_{DS}(\Delta) = \begin{cases} 0.65 & ; \Delta < 10^{-4}(\text{smooth}) \\ (29 + 4 \cdot \log_{10}(\Delta))/20 & ; 10^{-4} < \Delta < 10^{-2} \\ 1.05 & ; \Delta > 10^{-2}(\text{rough}) \end{cases} \quad (3.15)$$

In regards to the dock surface, Δ , which is defined as k/D , is smaller than 10^{-4} . Subsequently C_{DS} can be set to 0.65.

$\psi(K_C)$ is depended on the Keulegan Carpenter (KC) number.

$$\psi(K_C) = \begin{cases} C_\pi + 0.10(K_C - 12) & 2 \leq K_C < 12 \\ C_\pi - 1.00 & 0.75 \leq K_C < 2 \\ C_\pi - 1.00 - 2.00(K_C - 0.75) & K_C \leq 0.75 \end{cases} \quad (3.16)$$

Determining the KC numbers for all wave conditions applied in course of the model test, it turned out that the KC number does not exceed 0.7. So that

$$\begin{aligned} \psi(K_C) &= C_\pi - 1.00 - 2.00(K_C - 0.75) \\ &= 1.8 - 2K_C \end{aligned} \quad (3.17)$$

with

$$C(\pi) = 1.50 - 0.024 \cdot (12/C_{DS} - 10) \approx 1.3 \quad (3.18)$$

This means that the drag coefficient changes with the wave conditions. But since the model should be usable for all environmental conditions without changing every time the drag coefficient, the coefficients are fixed to their mean values.

Slender Element	C_D
<i>Vertical Elements</i>	
Structure	42000 Ns^2/m^3
Skirt	49000 Ns^2/m^3
<i>Horizontal Elements</i>	
Skirt 1-8	30622 Ns^2/m^3

Table 3.4: Set drag coefficients

The impact of this simplification is further discussed in Section 5.1 .

3.3 Second Approach

3.3.1 Introduction to WAMIT model

In the second approach, the WAMIT model is established on basis of an example from the WAMIT Manual version 7.2 (see Figure 3.8 and Appendix C).

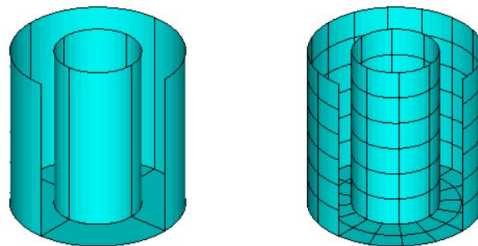


Figure 3.8: Cylinder with moonpool - Example 17a [21]

In the example, a circular cylinder with a concentric fluid chamber, referred to as a 'moonpool', is analysed. The cylinder consists of three patches; the inner, the outer wall and the bottom. An additional patch is introduced by a flexible lid located on the free surface of the moonpool. This lid accounts for viscous damping stemming from flow separation at the outer and inner corners of the cylinder. It basically damps the heave motions of the

cylinder. In order to accomplish that, two modes are defined for the lid; heave and pitch mode. More modes are not needed to get sufficiently accurate results. The body consisting of cylinder and lid has consequently eight DOFs.

1	surge	}	dock
2	sway		
3	heave		
4	roll		
5	pitch		
6	yaw		
7	heave	}	lid
8	pitch		

Table 3.5: DOFs in WAMIT

3.3.2 Calibration of WAMIT model

In the WAMIT example, a cylinder with a draft of 1m, an outer radius of 0.5m and an inner radius of 0.25m is used. The cylinder also does not have a skirt at its bottom. To be able to use the WAMIT example for the floating dock case, some calibrations and changes need to be done. First of all, the geometric data file from the example is updated based on the geometric data file created already for the first approach (see Subsection 3.2.1). Also the mass matrix and the damping matrix are changed in the force control file. The mass matrix is set to the values calculated in the first approach (see Subsection 3.2.2) and the damping matrix is established with regards to the model test results. Besides that, some smaller changes are done in the configuration file. For example, the panel size is adjusted to 16 and the sub-panel size to 5x5. In this way, the computing work is reduced while the accuracy remains steady. The WAMIT input files with all calibrations established can be found in Appendix D. After calibrating the files, the analysis is run in WAMIT.

3.3.3 Input to SIMA

Using the first approach, no changes had to be done to the WAMIT output file before importing it to SIMA. Using now the second approach, some manipulations have to be done.

In WAMIT, the model only consisted of one single body with eight DOFs. SIMA, however, can not handle bodies with more than six DOFs. To work around this problem, the single body is divided into two separate bodies; the dock and the lid. The dock has six DOFs as usual, but the lid only has two DOFs (heave and pitch mode). The remaining DOFs of the lid are dummy modes. To keep firm with the order of the DOFs, the heave mode of the lid is set to the surge position (1) and the pitch mode is set to the sway position (2).

WAMIT		SIMA		
1	surge	1	surge	} dock
2	sway	2	sway	
3	heave	3	heave	
4	roll	4	roll	
5	pitch	5	pitch	
6	yaw	6	yaw	
7	heave	1	surge	} lid
8	pitch	2	sway	
		3	heave	
		4	roll	
		5	pitch	
		6	yaw	

Table 3.6: Corresponding DOFs in SIMA

It is important to keep the order of the DOFs in mind, when assessing the results of the SIMA analysis. If for example one examines the surge-surge transfer function between dock and lid, it is actually the surge-heave transfer function between dock and lid.

3.3.4 Modification in SIMA

After the manipulated output file is imported to SIMA, several other modifications are established. First of all the mass properties of the bodies are adjusted. The moments of inertia and the mass of the lid are set to infinitesimal small values. In this way, the calculations are not distorted but SIMA can handle the body. Also a mooring system is added to the model. It is established by four horizontal fixed force elongations (springs) having the same characteristics as the mooring lines in the model tests (see also Subsection 3.2.2 'Calibration of WAMIT model'). The lines are attached to the dock at $z = -55\text{m}$ so that the model can rotate freely around its center of gravity (see Figure 3.9). The fixed force elongations are chosen in the second approach to model the mooring system because they have proven to reflect reality better. Moments inside the springs are directly calculated by SIMA and the stress curve of the lines can be determined.

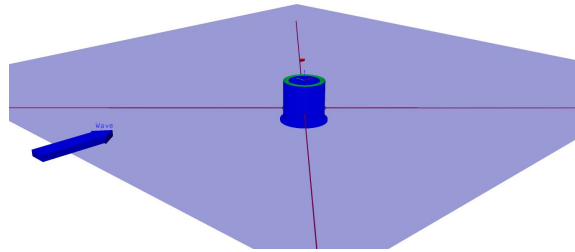


Figure 3.9: Model in SIMA

In addition to the mooring lines, two vertical slender elements are added to the model: one for the dock and one for the skirt. They have the same drag coefficients as calculated in Section 3.2.4 'Modification in SIMA'. Horizontal slender elements are not included since the lid already accounts for viscous effects at the outer and inner corners of the skirt. Finally the linear damping of the dock is adjusted so that peaks from the mooring system are damped out.

Chapter 4

Analysis

In the previous section, two numerical approaches to simulate the floating dock were presented. In this section, the results of their implementation are discussed and evaluated.

Three different types of simulations are run: simulations under regular wave conditions, decay tests and simulations under irregular wave conditions. The regular wave conditions are the same as in the model tests (see Appendix B) so that their results can be compared. The comparison is done with regards to the RAOs. The decay tests are conducted to identify the natural periods of the dock model and the simulations under irregular wave conditions are run to find the limiting sea states of the dock model.

4.1 Regular Wave Conditions

The assessing of the regular wave conditions is done in two separate steps. First the actual time series are inspected. Then the RAOs are calculated and the plots of the two approaches are compared among each other.

4.1.1 Time series

When applying regular waves on the dock, a regular response is expected. The period of the response should be equal to the wave period and the amplitude of the response should be constant over the time interval. The following figures show the global total position over time of some of the regular wave conditions for both approaches.

First a plot with curve progression as expected is presented. After that plots with conspicuous curve progression are evaluated. For the first approach, conditions with wave periods

of 9s in surge (Figure 4.2), 13s in heave (Figure 4.3), 17s in pitch (Figure 4.1), 21s in surge (Figure 4.4) and 23s in pitch (Figure 4.5) are chosen to be discussed more closely.

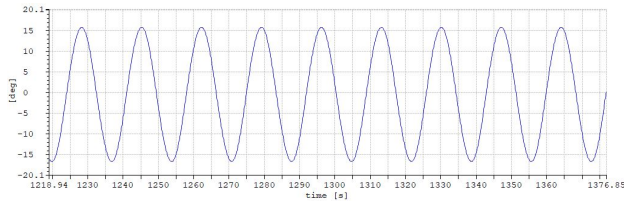


Figure 4.1: Dock motion in pitch at wave period of 17s

The dock motion in pitch at a wave period of 17s is a perfect example of how the dock is expected to behave. The response period is equal to the wave period of 17s and the amplitude is constantly at around 15°.

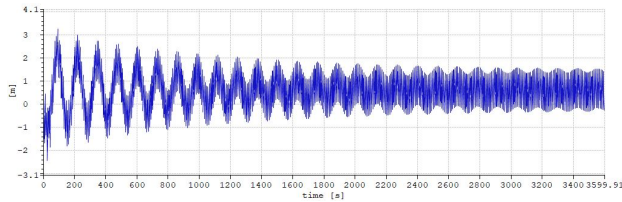


Figure 4.2: Dock motion in surge at wave period of 9s

One of the unexpected issues, that occurred in the time series, is large oscillation arising at lower wave periods in surge. The oscillation has a period of around 150s and damps smoothly out over time.

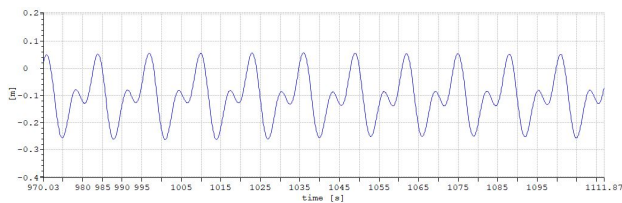


Figure 4.3: Dock motion in heave at wave period of 13s

Another unexpected issue is that the response period amounts half the wave period for some conditions in heave. The reason for this, however, can be found in the location of the reference point and the center of gravity. The reference point in SIMA is located at (0,0,0). Whereas the center of gravity of the dock is set to (0,0,-55). So when the dock fulfills one cycle in pitch around the center of gravity, the reference point moves meanwhile up and down twice. Adding those movement to the actual heave motion gives a curve with halved

excitation period. The smaller peaks indicate hereby the peaks of the pitch motion. When calculating the RAOs, the halved period can easily be filtered out by a low-pass filter.

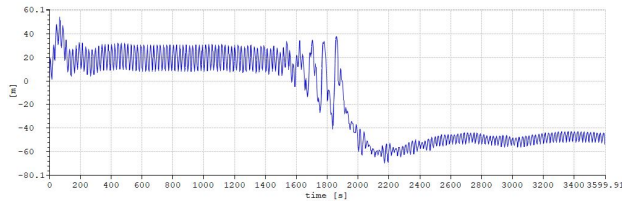


Figure 4.4: Dock motion in surge at wave period of 21s

At most of the wave conditions, the mean value in surge, heave and pitch shifts away from zero directly after the simulation started. But for surge and pitch at conditions with wave periods higher than 18s, the mean shifts a second time. This can be seen in the figures above and below. After the shift, the amplitude of the oscillation changes as well and in case of pitch motion even the response period changes (see figure below). Those issues crystallise as main problem in the first approach.

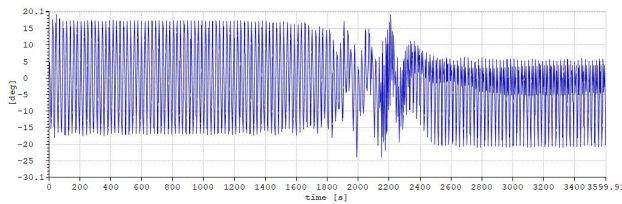


Figure 4.5: Dock motion in pitch at wave period of 23s

For the second approach, less problems occurred. Only conditions with wave periods of 9s in heave (Figure 4.8), 15s in pitch (Figure 4.6) and 21s in surge (Figure 4.7) are chosen to be discussed more closely.

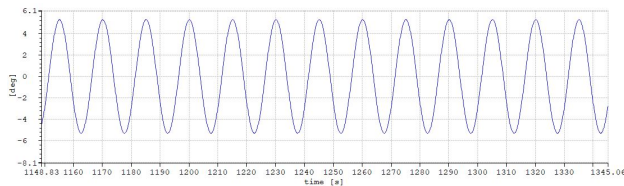


Figure 4.6: Dock motion in pitch at wave period of 15s

The figure above shows the dock motion in pitch at a wave period of 15s. Like for the first approach, this plot should visualize how the motion is expected to oscillate: with a constant amplitude and a period equal to the wave period.

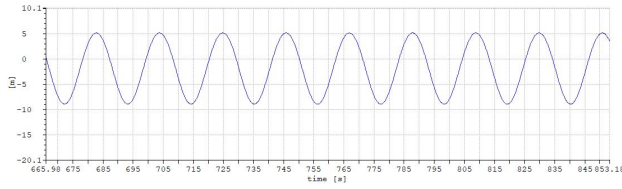


Figure 4.7: Dock motion in surge at wave period of 21s

In surge at a wave period of 21s, a mean value unequal to zero can be detected. A shifted mean value can be found in most of the curve progressions in surge, heave and pitch. The shift occurs in dependency with the retardation function and the time step with which it is imported. The shift can be filtered out in the PostProcessor of SIMA.

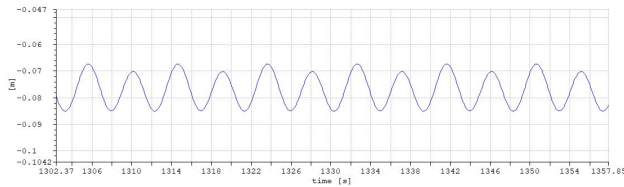


Figure 4.8: Dock motion in heave at wave period of 9s

Figure 4.8 gives an example for an issue that occurred already at the first approach. The response period is equal to half the excitation period. As already mentioned above (see Figure 4.3), this is due to heave-pitch coupling and is no sign of an erroneous model.

4.1.2 Response Amplitude Operators

On basis of the time series, the RAOs of the models can be established (see also Section 2.3 'Response Amplitude Operator'). For some wave conditions, the RAO was rather difficult to determine. Those RAOs are marked with a red circle in the plots. The data of the model tests are not to be published to the current point of time which is why they do not appear in the plots. However, all optimizations are done in regards to them.

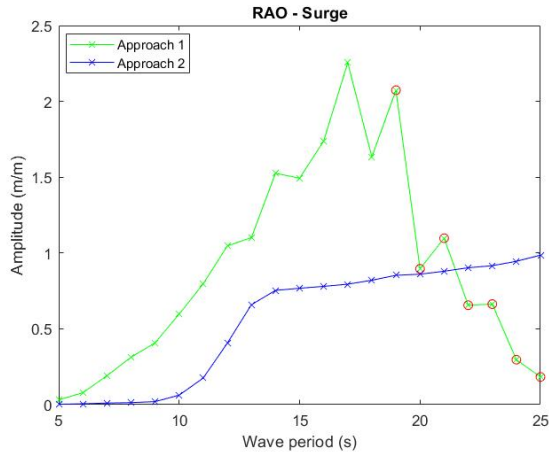


Figure 4.9: RAOs in surge for the first and second approach

Figure 4.9 shows the RAOs in surge. Peaks are expected to arise at around 7s and 20s since those are the natural periods in sloshing and piston mode of the dock. However, no peaks can be located in that regions. The first approach shows one peak at around 17s, while the second approach shows no proper peak at all. Nevertheless, the plot of the second approach gets close to the plot of the model tests. Especially at wave periods of 5-6s, 8-11s and 21-25s, the second approach gives a very good approximation for the RAOs of the model tests. The first approach on the contrary differs quite much from the plot of the model test. The response of the numerical model is much higher than expected.

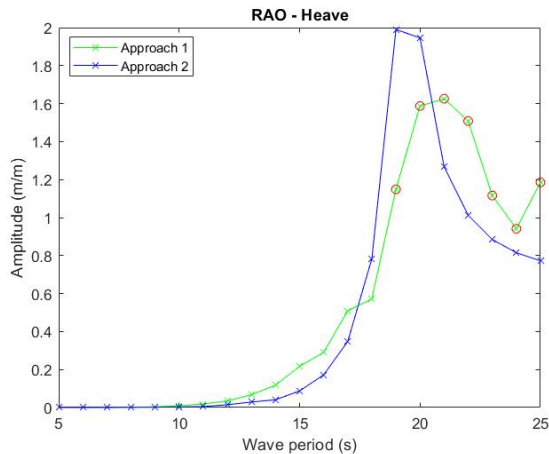


Figure 4.10: RAOs in heave for the first and second approach

The RAO curve progression in heave should be dominated by the piston mode of the

dock. In the model tests, the piston mode occurred at around 20s. In Figure 4.10, both approaches show peaks at around this period: the first approach at 21s, the second at 19s. Also up to 20s, the slopes of both approaches come quite close to the slope of the model test. However, the absolute values of the peaks differ from each other to a fair extent. In addition to that, the RAOs of both approaches decrease fast after they peaked. In the model tests, the response stays nearly constant after its peak at 20s.

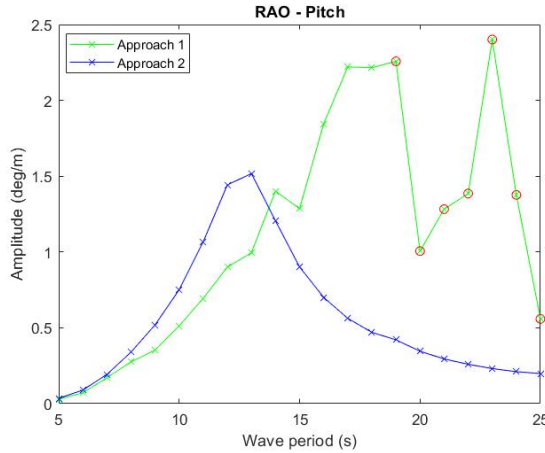


Figure 4.11: RAOs in pitch for the first and second approach

For the RAOs in pitch, both modes, sloshing and piston mode, should be clearly visible in the curve progression. But both approaches differ noticeably from the model tests (see Figure 4.11). The first approach has one peak at around 18s wave period and another at 23s. The second peak might occur hereby due to difficulties in determining the RAOs. The second approach has only one peak at around 13s. That is an unexpected shift of 7s. Also the absolute values of the peaks do not match the absolute value of the peak in the model test. These differences might indicate that there are still some issues with the coupling of the mooring system and the dock (see also Section 6.2 'Recommendation for future work').

Comparing all RAOs, determined from the model tests, the first and second approach, shows clearly that the second approach is much more realistic than the first one. At the second approach, the absolute values are closer to the ones from the model tests and also the curve progression is smoother than at the first approach. At the first approach, the odd course of the time series made it partly difficult to read off the correct RAO which is another reason why the second approach is preferable. So for further tests and evaluations, only the second approach is pursued.

4.2 Decay Tests

Decay test analyses are performed in order to document the system's natural periods and damping. In this case, the damping is already known from calculations in WAMIT, so that only the natural period of the dock is desired. Also only surge, heave and pitch need to be considered since the dock is point symmetric.

Each decay test is subdivided in three phases. In the first one, a ramp force or moment is applied to the dock. The ramp force/moment starts at zero and increases over time until it reaches the desired value. In the second one, the force/moment is held constantly at this value until the third phase starts and the force/moment is removed from the dock. The direction vector of the force/moment differs depending on whether surge, heave or pitch is considered. In surge the force acts in negative x-direction, in heave the force acts in negative z-direction and in pitch the moment acts anti-clockwise round the y-axis.

So in the first phase, the dock is moved smoothly in a new position. In the second, this position becomes static. And in the third one, the dock is released and oscillates slowly back to its initial position. The oscillation period is hereby the natural period in surge, heave or pitch depending on the direction vector. That is because the differential equation describing the motions is:

$$(M + A)\ddot{x} + B\dot{x} + Cx = 0 \quad (4.1)$$

where M is the mass, A the added mass, B the damping and C the restoring stiffness. The natural frequency of the undamped system is thus given as:

$$\omega_0 = \sqrt{\frac{C}{M + A}} \quad (4.2)$$

$$T_0 = 2\pi\sqrt{\frac{M + A}{C}} \quad (4.3)$$

For the decay test in surge, a force of $5 \cdot 10^6 N$ is specified in negative x-direction. It is applied at the CoG of the dock so that the model experiences no moment. The force is built up in the phase from 50 to 150s. It is then kept constant from 150 to 350s. After 350s the force is released and the dock starts to oscillate with its natural period in surge. The dock is back in its initial position after around 700s.

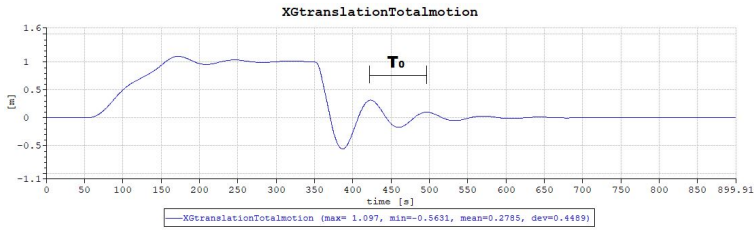


Figure 4.12: Decay test in surge

With regards to Figure 4.12 above, the natural period in surge for the dock model is 75s. Since no decay tests were conducted for the physical model, this value can only be compared to results of other numerical models.

Zhiyu Jiang created a dock-spar model in SIMA for the hydrodynamic load and motion analyses he is working on (see Section 3.1 'Previous Work'). His model bases on the latest values of the optimization (see Table 3.1) and the mooring system is a catenary system consisting of four chains, which are tangentially attached to the sea floor. To be able to compare both models, the catenary system is replaced by the fixed force elongations used in the current model. Having modified the other numerical model like this, the same decay test in surge is conducted. It results in a natural period of 70s, which is close to the result from the current model. The deviation of 5s may stem from the dimension variation.

For the decay test in heave, a force of $6 \cdot 10^7 N$ is specified in negative z-direction at the CoG of the dock. The ramp and constant force phases are somewhat shorter than at the decay test in surge: 50s and 100s. This is because the added mass in surge is higher than in heave.

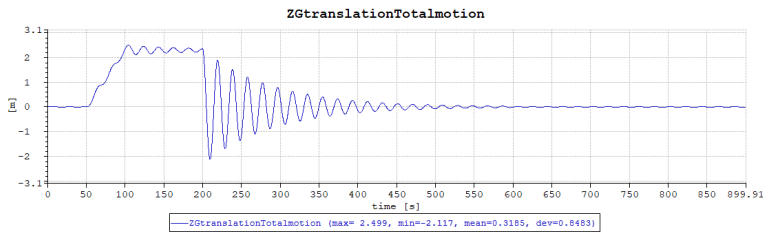


Figure 4.13: Decay test in heave

Figure 4.13 shows that the natural period in heave of the dock is 20s. The value is again compared to the modified model of Zhiyu Jiang. His model shows a natural period in heave of 20s. So that it fully confirms the result of the current model.

For the decay test in pitch, a moment of $1 \cdot 10^{10} Nm$ is specified anti-clockwise round the y-axis at the CoG of the dock. The ramp and constant moment phases are the same as at the decay test in heave.

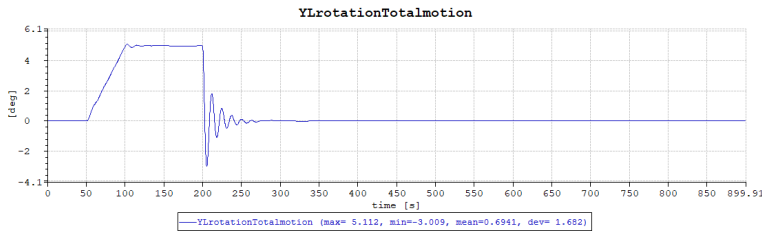


Figure 4.14: Decay test in pitch

Figure 4.14 shows that the natural period in pitch of the dock is 12.5s. The modified model of Zhiyu Jiang gives a natural period in pitch of 12s. So that all in all, the decay results of the current model are confirmed by the results of the modified model.

4.3 Irregular Wave Conditions

The irregular wave conditions are chosen with regards to two different modes of the dock: the operational and the survival mode. In the operational mode, significant wave heights of around 2-3m and peak periods of 9-13s are expected. In those wave conditions, the dock should only have limited movements. The OWTs are assembled inside the dock during those environmental conditions and the components as well as the workers should not be negatively effected by the dock's motion.

The wave parameters in survival mode are chosen based on a Metocean Design Basis Report of Equinor [23]. The report was established for the Staffjord oil field located in the U.K.-Norwegian boundary of the North Sea. The Metocean data of this location should reflect the environment of the floating dock in an acceptable way. The water depth of the field is 145m and the North Sea is one of the area of applications of the dock.

Since the dock will only be at the site for the duration of the WT installation, an extreme sea state with a return period of one year is chosen. So that for the survival mode of the dock, wave conditions with a significant wave height of 11m and a peak period of 14.2s are applied with a duration of 3 hours.

Figures 4.15, 4.16, 4.17, 4.18, 4.19, 4.20, 4.21 and 4.22 on the next two pages show exemplary the response and wave spectrum of the lowest operational mode and the survival mode.

- $H_s=2m, T_p=9s$

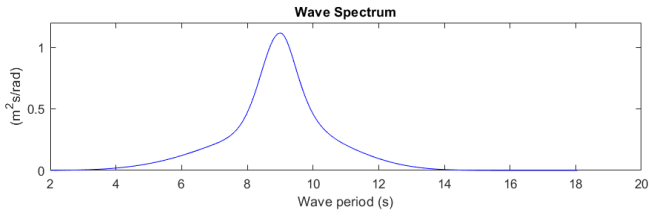


Figure 4.15: Operational mode - Wave spectrum

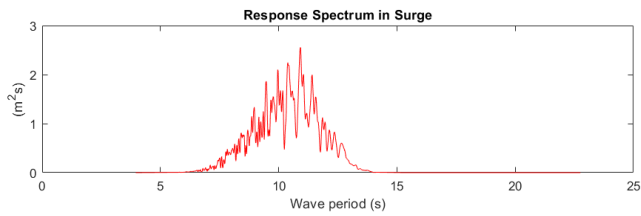


Figure 4.16: Operational mode - Response spectrum in surge

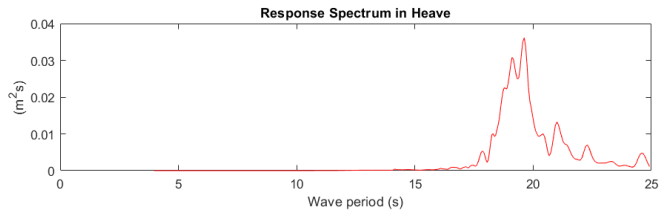


Figure 4.17: Operational mode - Response spectrum in heave

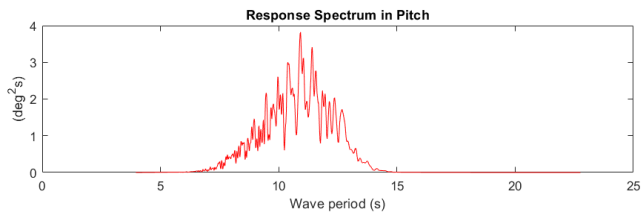


Figure 4.18: Operational mode - Response spectrum in pitch

- $H_s=11\text{m}$, $T_p=14.2\text{s}$

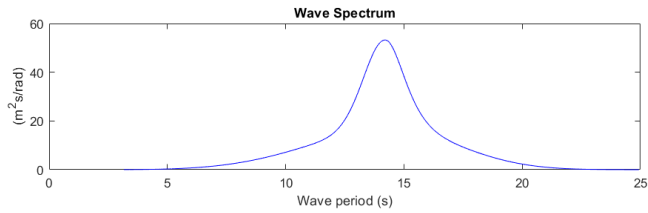


Figure 4.19: Survival mode - Wave spectrum

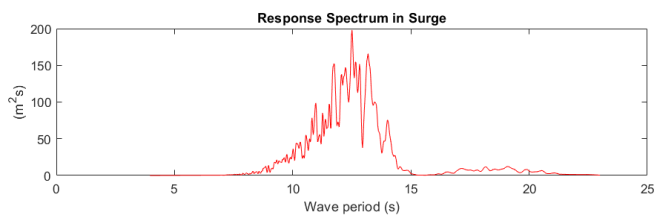


Figure 4.20: Survival mode - Response spectrum in surge

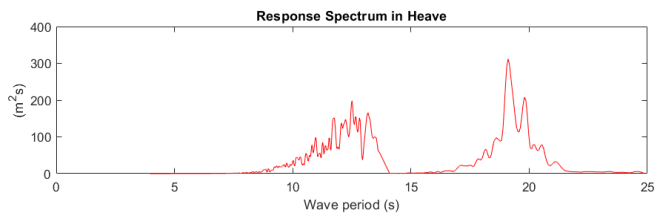


Figure 4.21: Survival mode - Response spectrum in heave

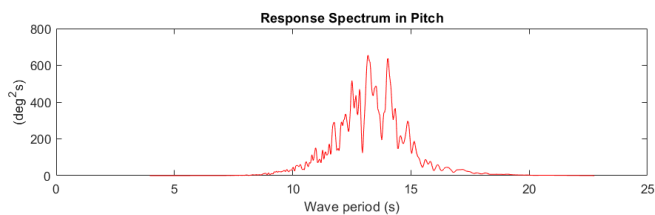


Figure 4.22: Survival mode - Response spectrum in pitch

The wave spectra of both conditions are JONSWAP spectra built up on two parameters; the significant wave height and the peak period of the sea state. The advantage of using a JONSWAP spectrum is that its form is very general and flexible [24]. It works for any sea state and SIMA simplifies the parameterisation to a great extent.

The response spectra of both conditions confirm clearly the results of the decay tests. Especially in pitch, both graphs show a definite peak at the natural period of 12.5s. In heave, a peak arises at the natural period of 20s. But in survival mode, there is another peak at around 12s. The second peak lines up with the peak in surge. No second peak accrues in surge since its natural period is at 75s. The wave spectrum, however, only includes waves with a period of up to 25s.

To determine the maximum motions and velocities that occur in operational and survival mode, ten simulations are run per sea state (see Appendix E). For the operational mode, three additional sea states are tested. Based on the gained values, the maximum motions and velocities of the dock are derived. They are stated in Table 4.1 and 4.2 below.

	surge [m]	heave [m]	pitch [deg]
<i>operational mode</i>			
$H_s=2m, T_p=9s$	0.826	0.056	1.00
$H_s=2m, T_p=13s$	1.273	0.347	1.90
$H_s=3m, T_p=9s$	1.235	0.124	1.49
$H_s=3m, T_p=13s$	1.901	0.523	2.84
<i>survival mode</i>			
$H_s=11m, T_p=14.2s$	6.179	3.192	10.51

Table 4.1: Maximum motion

	surge [m/s]	heave [m/s]	pitch [deg/s]
<i>operational mode</i>			
$H_s=2m, T_p=9s$	0.225	0.015	0.27
$H_s=2m, T_p=13s$	0.322	0.098	0.50
$H_s=3m, T_p=9s$	0.337	0.033	0.40
$H_s=3m, T_p=13s$	0.482	0.151	0.75
<i>survival mode</i>			
$H_s=11m, T_p=14.2s$	1.669	1.021	2.84

Table 4.2: Maximum velocity

The tables show that the maximum motions and velocities in operational mode reach partly critical values. Spar and WT can not be mated under pitch motions larger than 2°. For a sea state of $H_s=3m$ and $T_p=13s$, pitch angles of over 2.8° are attained. For the other three tested sea states, the maximum pitch angle does not exceed 1.9°. Also the maximum motion in surge and heave is only limited in those wave conditions. So that the work activities in the dock will not be effected by the movement of the structure. The operational limit of the establish dock model is consequently around $H_s=3m$ and $T_p=13s$. However, the

operational limit of the actual dock might lie around other wave conditions, since the dimensions and the mooring system of the established model differ from the actual dock (see also Section 6.2 'Recommendation for future work').

In survival mode, the dock is exposed to fairly high maximum motions and velocities. The personnel on the dock must be evacuated in those wave conditions. However, the structure will not be flooded. Its freeboard will not fall below 14m.

$$F_0 - z_{max} - \tan(\theta_{max}) \cdot r_2 = 25m - 3.192m - \tan(10.51deg) \cdot 40m = 14.4m \quad (4.4)$$

F_0 = initial freeboard

z_{max} = maximum motion in heave

θ_{max} = maximum motion in pitch

r_2 = outer diameter dock

In addition to the movement of the dock, the forces in the mooring lines are examined.

	Maximum [N]
<i>operational mode</i>	
$H_s=2m, T_p=9s$	$6.621 \cdot 10^7$
$H_s=2m, T_p=13s$	$6.722 \cdot 10^7$
$H_s=3m, T_p=9s$	$6.684 \cdot 10^7$
$H_s=3m, T_p=13s$	$6.832 \cdot 10^7$
<i>survival mode</i>	
$H_s=11m, T_p=14.2s$	$7.786 \cdot 10^7$

Table 4.3: Positioning force

The mooring system of the current SIMA model represents the mooring system used in the model test. This system will of course not be used for the actual dock. So that the results of the simulation are only very limited transferable to reality. However, comparing the results to Table C1 in 'DNV-OS-E302: Offshore Mooring Chain' shows that the maximum forces in the mooring lines in SIMA would require a Grade R5 mooring chain with a diameter of 1.56m in reality.

The diameter is disproportionately large because of the pretension applied in the model tests. With a reduced pretension of $1 \cdot 10^7 N$, a diameter of only 0.634m would be required.

Chapter 5

Discussion

In this section, the modelling approach and the analytical results presented in Section 3 and 4 are further discussed and evaluated. Uncertainties and inaccuracies of the numerical model are stated. Also the reliability and validity of the analytical results are assessed. Furthermore it is discussed to which extent the results fulfill the initial aim of this thesis.

5.1 Modelling Approach

The main uncertainty in the modelling phase was the computation of the viscous effects on the dock. For the first approach, ten slender elements were added to the basic model: two vertical and eight horizontal ones. For the second approach, the horizontal elements were replaced by a lid on the free surface of the dock. The lid as well as the slender elements account in a simplified way for the viscous effects. The largest simplification done hereby is for the slender elements to assume a constant drag coefficient over all wave conditions. The influence of this simplification is assessed by conducting a brief sensitivity analysis for C_D .

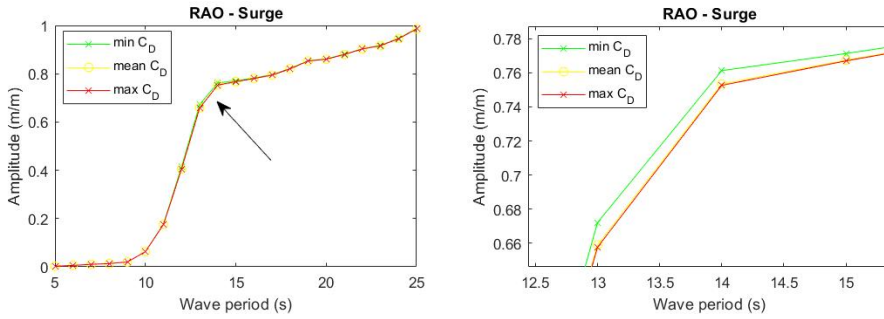


Figure 5.1: RAOs in surge for different C_D s

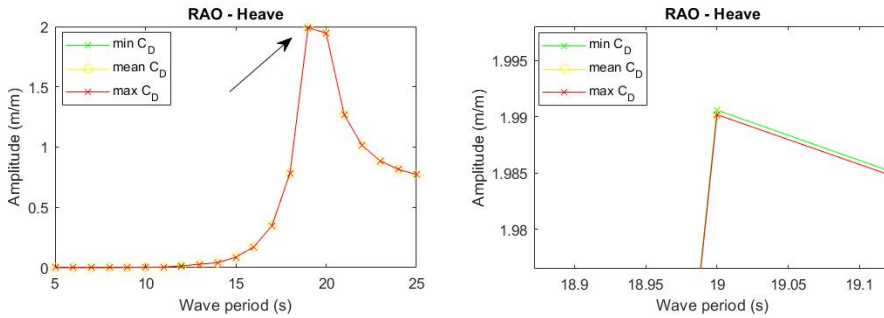


Figure 5.2: RAOs in heave for different C_D s

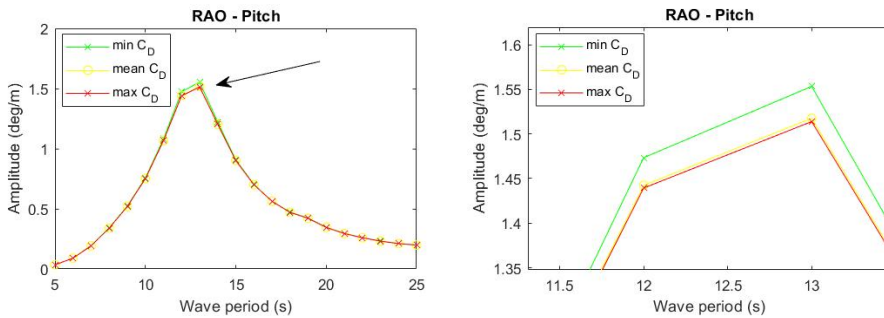


Figure 5.3: RAOs in pitch for different C_D s

For the first set of simulations, the C_D s are set to their minimum values. Those occur in the model tests at a wave period of 25s. For the second set of simulations, the C_D s are set to their maximum values which occur at a wave period of 5s. Both sets are then compared to the actual RAO plot with the C_D s set to their mean values. As it can be seen in Figure 5.1, 5.2 and 5.3, the influence of a varying C_D is limited. In surge, the maximum deviation

of RAOs occurs at a wave period of 13s and amounts 1.99%. In heave, it is only 0.02% at a wave period of 19s. And in pitch the maximum deviation is 2.36% at a wave period of 13s. A change of 2.36% at a wave period of 13s corresponds to a change in pitch angle of 0.16°.

Thus setting C_D to a constant value is an acceptable simplification. However, when interpreting the results of the simulations, one should keep in mind that there is an uncertainty in the calculated values.

The main inaccuracy in the modelling phase was the simplification of the mooring system. Assuming horizontal fixed force elongations instead of sloped mooring lines affects the pitch as well as the heave behaviour of the dock. The impact of the simplification becomes evident in the analytical results (see following section). However the horizontal alignment of the lines is indispensable. SIMA could not handle ascending fixed force elongations or ascending catenary lines.

5.2 Results of Analyses

The comparison of the RAOs in Section 4.1.2 'Response Amplitude Operators' shows that the numerical model still differs from the physical model to some degree. Especially the dock's behaviour in pitch is not accurately captured by the SIMA model. This might be due to the simplified mooring system in SIMA. However, the behaviour of the dock in surge and heave is acceptable close to the model test results. The dock model itself displays reality sufficiently. Replacing the mooring system of the model test by the mooring system of the actual dock should give results that realistically describe the behaviour of the structure in its operational mode. The initial aim of the thesis is met in that sense.

Of course, changing the mooring system affects the natural periods of the system as well as its limiting sea states. The natural periods determined in the decay tests of this thesis are only valid for the model test setup. Especially the natural period in surge will be much higher than 75s for the actual dock system. Also the natural period in pitch will increase, so that it will not interfere with the mating process of the OWTs. The natural period in heave, however, will presumably stay constant since it depends more on the geometry of the 'moonpool' than on the mooring system.

In any case, the decay tests as well as the irregular wave conditions have to be rerun and reevaluated for a changed mooring system.

Chapter 6

Conclusion

The conclusion is divided into two subsections. First the most important parts of the thesis are summarized then a recommendation for subsequent work is given. For the recommendation, the thesis is placed within a broader perspective, pointing out possibilities that arise from the thesis for the floating dock project.

6.1 Summary

Equinor proposed a floating dock concept for assembling spar floating wind turbines near the offshore wind farm site. The purpose of this thesis was to establish a numerical model which coincide with the results of conducted model tests and to examine the behaviour of the dock in its operational mode.

The numerical modelling was done in two separate steps. First the hydrodynamic problem was solved in frequency domain in WAMIT, a program that analyzes the interaction between ocean waves and offshore structures. Then, after the simulations had been run in WAMIT, the result files were imported to SIMA, a workbench that analyses marine operations and floating systems in time domain.

Two different modelling approaches were separately analysed. In the first approach the WAMIT input files were generated by a set of Matlab files compiled by Maël Moreau. They were further modified in regards to mass and stiffness properties to meet the model tests results. In the second approach the dock was modelled by four patches: one representing the inner wall, one the outer wall, one the bottom and one representing a lid on the inner free surface. The lid was very flexible and accounted for viscous damping stemming from flow separation at the outer and inner corners of the cylinder. Thus, it basically damped the heave motions of the cylinder.

The models of both approaches were further modified to bring them closer to the physical model. One of the modifications done in SIMA was the addition of slender elements. They induced drag forces which arise in reality from the cylindrical shape of the dock. Also the damping matrix of the structure and the mooring system were adjusted to improve the behaviour of the models. The behaviour was hereby assessed in terms of the non-dimensional RAO which was calculated by dividing the response amplitude (dock motion) by the excitation amplitude (wave amplitude).

Comparing the RAOs of the first approach, the second approach and the model tests showed clearly that the second approach was much more realistic than the first one. The absolute values were closer to the ones from the model tests and also the curve progression was smoother than at the first approach. At the first approach, some time series showed an odd course with shifted means and varying oscillations. So that only the second approach was pursued. It proven to acceptably reflect the dock motion in surge and heave. In pitch, however, there are still some discrepancies, presumably caused by the simplified mooring system.

Decay tests were run for the second approach. They gave natural periods of 75s in surge, 20s in heave and 12.5s in pitch. The pitch natural period coincided with the operational wave conditions. But since the mooring system will change for the actual dock, the natural period in pitch is expected to increase so that it will not interfere with the mating process of the OWTs. In addition to the decay tests, five irregular wave conditions were run ten times for the dock model. Four wave conditions described the operational mode of the dock, one the survival mode. The dock model proved to survive wave conditions with a return period of one year in the North Sea. The operational limits, however, occurred already around a significant wave height of 3m and a peak period of 13s due to a limit in pitch motion of 2° .

The main conclusion, that can be drawn from this thesis, is that the dock itself can be realistically modeled with its basic structure plus a lid on the free surface of the 'moonpool' and two vertical slender elements with constant C_D accounting for viscous effects. The mooring system, however, needs further modifications. Replacing it with the actual mooring system of the dock will change the system's natural periods and limiting sea states so that the given requirements for the dock are expected to be met.

6.2 Recommendation for future work

Based on the conclusion and based on the broader perspective of the project, future work could be to replace the mooring system of the current model by a catenary system that resembles the actual mooring system of the dock. Zhiyu Jiang introduced such a mooring system already to his SIMA model, so that the current dock model could be combined with the mooring system of Zhiyu Jiang's model (see Figure 6.1).

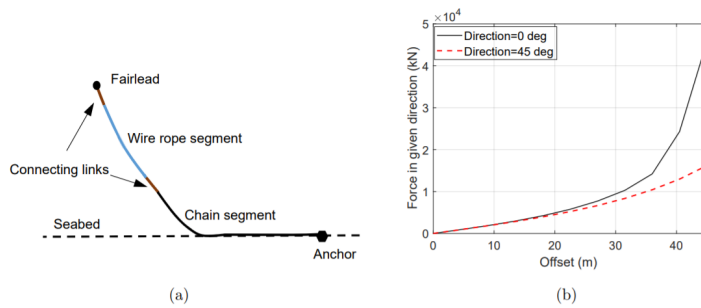


Figure 6.1: Mooring system of Zhiyu Jiang's model [25]

The dock itself is sufficiently calibrated and with the actual mooring system, realistic limiting sea states and prediction of behaviour could be found for the real-life dock.

Furthermore a spar body could be added to the system to analyse operations like the mating between spar and WT more closely.

Also the current SIMA model could be further modified to bring it even closer to the model test results. A special focus should lie hereby on the coupling between mooring system and dock.

Bibliography

- [1] International Energy Agency (IEA). *Key World Energy Statistics*. 2017. URL: <https://www.iea.org/publications/freepublications/publication/KeyWorld2017.pdf> (visited on 04/16/2018).
- [2] International Renewable Energy Agency (IRENA). *Wind energy*. 2018. URL: <https://www.irena.org/wind> (visited on 04/16/2018).
- [3] Erin Bachynski. "Introduction to offshore wind power and technology". In: *Norwegian University of Science and Technology* (Aug. 2018). Lecture slides - TMR4505 Marin konstruksjonsteknikk.
- [4] Erin Bachynski. "Offshore wind turbine installation and access systems". In: *Norwegian University of Science and Technology* (Oct. 2018). Lecture slides - TMR4505 Marin konstruksjonsteknikk.
- [5] Lin Li. "Dynamic Analysis of the Installation of Monopiles for Offshore Wind Turbines". In: *Norwegian University of Science and Technology* (2016).
- [6] DNV GL. *Engineering analysis of fixed and floating OWT structures - Sesam for offshore wind*. 2016. URL: <https://www.dnvgl.co.kr/services/engineering-analysis-of-fixed-and-floating-owt-structures-sesam-for-offshore-wind-2438> (visited on 10/30/2018).
- [7] Frederick Driscoll et al. "Validation of a FAST Model of the Statoil Hywind Demo Floating Wind Turbine". In: *Energy Procedia* 94 (Sept. 2016), pp. 3–19. DOI: 10.1016/j.egypro.2016.09.181.
- [8] Equinor ASA. *How Hywind works*. 2018. URL: <https://www.equinor.com/en/what-we-do/hywind-where-the-wind-takes-us/hywind-up-close-and-personal.html> (visited on 10/25/2018).
- [9] 4C Offshore. *Hywind - Demo Offshore Wind Farm*. 2016. URL: <https://www.4c offshore.com/windfarms/hywind---demo-norway-no04.html> (visited on 10/25/2018).
- [10] Equinor ASA. *Hywind - the worlds leading floating offshore wind solution*. 2018. URL: <https://www.equinor.com/en/what-we-do/hywind-where-the-wind-takes-us.html> (visited on 10/25/2018).

-
- [11] Tom Russell. *Last Hywind turbine arrives in Scotland*. 2017. URL: <https://www.4coffshore.com/windfarms/last-hywind-turbine-arrives-in-scotland-nid6270.html> (visited on 10/30/2018).
- [12] Yngve Børstad. *Hywind Scotland Pilot Park - Marine Operations*. 2016. URL: <http://www.subops.no/content/uploads/2016/05/Yngve-Borstad.pdf> (visited on 10/30/2018).
- [13] Nathalie Thomas. *Worlds first floating wind farm towed to North Sea base*. 2017. URL: <https://www.ft.com/content/2050b1de-72bc-11e7-aca6-c6bd07df1a3c> (visited on 12/10/2018).
- [14] Jannicke Nilsen. *Sjekk dimensjonene: Disse kjettingene skal feste Statoils flytende vindmølle til havbunnen*. 2016. URL: <https://www.tu.no/artikler/sjekk-dimensjonene-disse-kjettingene-skal-feste-statoils-flytende-vindmolle-til-havbunnen/346472> (visited on 10/30/2018).
- [15] Joshua S. Hill. *Hywind Scotland, Worlds First Floating Wind Farm, Performing Better Than Expected*. 2018. URL: <https://cleantechnica.com/2018/02/16/hywind-scotland-worlds-first-floating-wind-farm-performing-better-expected/> (visited on 10/25/2018).
- [16] Equinor ASA. *Worlds first floating wind farm has started production*. 2017. URL: <https://www.equinor.com/en/news/worlds-first-floating-wind-farm-started-production.html> (visited on 10/28/2018).
- [17] Zhen Gao. “Marine Operations Related to Installation of Offshore Wind Turbines”. In: *Norwegian University of Science and Technology* (Oct. 2018). Presentation at the Ocean University of China.
- [18] Georgios Nikitas Subhamoy Bhattacharya and Saleh Jalbi. “On the Use of Scaled Model Tests for Analysis and Design of Offshore Wind Turbines”. In: *Geotechnics for Natural and Engineered Sustainable Technologies, Developments in Geotechnical Engineering* (Feb. 2018).
- [19] Odd M. Faltinsen and Oleksandr Tymocha. *Sloshing*. Cambridge University Press, 2009, pp. 1–4, 27–30, 103–110. ISBN: 9781107646735.
- [20] Odd M. Faltinsen. *Sea Loads on Ships and Offshore Structures*. Cambridge University Press, 1990. ISBN: 0521458706.
- [21] Inc. WAMIT. “WAMIT USER MANUAL Version 7.2”. In: (2016).
- [22] Chittiappa Muthanna. “General Modelling and Scaling Laws”. In: *Norwegian University of Science and Technology* (Aug. 2018). Lecture slides - TMR7 Experimental Methods in Marine Hydrodynamics.
- [23] Kenneth J. Eik and Einar Nygaard. “Statfjord Late Life Metocean Design Basis”. In: (Dec. 2003). Document no.: PTT-NKG-RA 0044.
- [24] Bernard Le Mehaute and Daniel M. Hanes. *Global Coastal Ocean - Multiscale Interdisciplinary Processes*. Ocean Engineering Science - Volume 9. Harvard University Press, 2005. ISBN: 0674017390.
- [25] Zhiyu Jiang et al. “Concept development of a large floating dock for spar floating wind turbine installation”. In: (May 2019).
- [26] Zhiyu Jiang. “Brief on the floating dock project”. In: *Norwegian University of Science and Technology* (July 2018).
-

Appendix

Appendix A

Design constraints (nonlinear)

1. Initial stability in operation ($GMO > 1.0$ m)
2. Initial stability in transit (**$GMT > 1.0$ m**)
3. Limitation of ballast in operation ($H_{bwo} + H_{bf} < T_o + F_o$)
4. Limitation of ballast in transit ($H_{bwt} + H_{bf} < T_t + F_t$)
5. Piston-mode resonance criteria in operation ($T_{no} > 17$ s)
6. Wind-induced heeling angle in operation ($\eta_{5o} \leq 2$ deg)
7. Wind-induced heeling angle in survival ($\eta_{5s} \leq 7$ deg)
8. Wind-induced heeling angle in transit ($\eta_{5t} \leq 2$ deg)
9. Heave natural period ($T_{n3} > 25$ s) NOT IMPLEMENTED
10. Pitch natural period ($T_{n5} > 25$ s) NOT IMPLEMENTED

Figure 6.2: Design constraints [26]

Shallow dock constraints (linear)

1. Range of draft in operation, T_o [50, 100] m
 2. Range of draft in transit, T_t [5, 20] m
- Note: the max. depth of Suez canal is **20.1** m !
3. Variation in breadth of upper deck ($10 < D - d < 100$ m)
 4. Range of fixed ballast height, H_{bf} [5, 25] m
 5. Range of freeboard in operation, F_o [15, ∞] m
 6. Range of outward bilge tank, B_{osk} [6, 15] m
 7. Range of inward bilge tank, B_{isk} [0, $(d-25)/2$] m
 8. Range of bilge tank height, H_{sk} [4, 8] m

Figure 6.3: Shallow dock constraints [26]

Appendix B

Table 6.1: Model tests - Wave periods

Wave periods (s)		
<i>Set 1</i>	<i>Set 2</i>	<i>Set 3</i>
0.503187956	0.604184784	1.519097294
0.507192663	0.609740979	1.541354466
0.511294533	0.615453336	1.564619516
0.515497561	0.621329309	1.588970884
0.519805974	0.627376862	1.614495827
0.524224251	0.633604511	1.641291745
0.528757143	0.640021375	1.669467741
0.53340969	0.646637235	1.699146498
0.538187253	0.653462594	1.730466531
0.543095533	0.660508745	1.763584915
0.5481406	0.667787857	1.79868061
0.553328929	0.675313055	1.835958543
0.55866743	0.683098526	1.875654664
0.564163492	0.691159627	1.918042256
0.569825019	0.699513016	1.963439894
0.575660485	0.708176793	2.012221571
0.581678983	0.71717067	2.064829748
0.587890285	0.726516155	2.121792366
0.59430491	0.736236773	
0.600934199	0.74635831	
0.607790398	0.756909106	
0.614886755	0.767920386	
0.622237624	0.779426653	
0.629858594	0.791466138	
0.63776662	0.804081339	
0.645980189	0.817319653	
0.654519495	0.831234126	
0.663406656	0.845884349	
0.672665947	0.861337535	
0.682324086	0.877669819	
0.692410556	0.894967842	
0.702957981	0.913330693	
0.714002576	0.932872302	
0.725584669	0.953724431	
0.73774932	0.976040428	
0.750547061	1	
Continued on next page		

Table 6.1 – continued from previous page

Wave periods (s)		
<i>Set 1</i>	<i>Set 2</i>	<i>Set 3</i>
0.764034785		
0.778276805		
0.793346155		
0.809326169		
0.826312425		
0.844415163		
0.863762305		
0.884503285		
0.906813925		
0.930902756		
0.957019271		
0.985464895		
1.016607763		
1.050902984		
1.088920979		
1.131387993		
1.179245469		
1.233739647		
1.296561439		
1.370073694		
1.457698734		
1.564619516		
1.699146498		
1.875654664		
2.121792366		
2.5		

Table 6.2: Model tests - Wave periods and heights in full scale

Wave periods (s)			Wave heights (m)		
<i>Set 1</i>	<i>Set 2</i>	<i>Set 3</i>	<i>Set 1</i>	<i>Set 2</i>	<i>Set 3</i>
5.031879563	6.04184784	15.19097294	0.616253148	0.814864139	0.060049455
5.071926627	6.09740979	15.41354466	0.624241628	0.825591986	0.061821984
5.11294533	6.154533357	15.64619516	0.632416919	0.836599112	0.063702338
5.154975611	6.213293091	15.88970884	0.640785864	0.84789815	0.065700665
5.198059743	6.273768622	16.14495827	0.649355695	0.859502588	0.067828426
5.242242514	6.336045109	16.41291745	0.658134068	0.871426853	0.070098619
5.287571426	6.400213754	16.69467741	0.667129092	0.883686388	0.072526038
5.334096904	6.466372355	16.99146498	0.676349368	0.896297752	0.075127604
5.381872534	6.534625937	17.30466531	0.685804029	0.909278722	0.077922755
5.430955327	6.605087453	17.63584915	0.695502784	0.922648414	0.080933932
5.481405998	6.67787857	17.9868061	0.705455965	0.936427412	0.084187186
5.533289285	6.753130553	18.35958543	0.715674582	0.950637919	0.087712932
5.586674301	6.83098526	18.75654664	0.726170386	0.965303923	0.091546902
5.641634915	6.911596271	19.18042256	0.736955926	0.980451387	0.09573136
5.698250188	6.995130155	19.63439894	0.748044632	0.996108462	0.100316671
5.756604849	7.081767928	20.12221571	0.759450889	1.012305728	0.10536333
5.816789826	7.171706698	20.64829748	0.77119013	1.029076475	0.110944654
5.878902845	7.265161552	21.21792366	0.783278935	1.046457017	0.117150363
5.943049098	7.362367727		0.795735149	1.064487055	
6.00934199	7.463583096		0.808578004	1.083210094	
6.077903982	7.569091057		0.82182826	1.102673925	
6.148867548	7.679203865		0.835508372	1.122931185	
6.222376245	7.794266532		0.849642667	1.144040009	
6.298585941	7.91466138		0.864257551	1.166064789	
6.377666203	8.040813391		0.879381743	1.18907707	
6.459801885	8.173196533		0.895046545	1.213156607	
6.54519495	8.312341262		0.911286143	1.238392615	
6.634066555	8.458843491		0.928137966	1.264885271	
6.72665947	8.613375347		0.945643083	1.292747505	
6.823240864	8.776698187		0.963846679	1.322107175	
6.924105556	8.949678423		0.982798595	1.353109699	
7.029579805	9.133306929		1.002553969	1.385921301	
7.140025758	9.328723018		1.023173977	1.420732994	
7.255846687	9.537244307		1.044726717	1.457765565	
7.377493196	9.760404281		1.067288242	1.497275824	
7.505470615	10		1.090943802	1.539564545	
7.640347849			1.115789327		
7.782768051			1.141933207		
7.933461555			1.169498462		
8.093261693			1.198625376		

Continued on next page

Table 6.2 – continued from previous page

Wave periods (s)			Wave heights (m)		
<i>Set 1</i>	<i>Set 2</i>	<i>Set 3</i>	<i>Set 1</i>	<i>Set 2</i>	<i>Set 3</i>
8.263124253			1.229474759		
8.444151625			1.262231969		
8.63762305			1.297111967		
8.845032847			1.33436569		
9.068139254			1.374288199		
9.309027558			1.417229198		
9.570192708			1.463606799		
9.854648954			1.513925779		
10.16607763			1.568802175		
10.50902984			1.628997007		
10.88920979			1.69546339		
11.31387993			1.769413877		
11.79245469			1.852419099		
12.33739647			1.946556548		
12.96561439			2.054642752		
13.70073694			2.180610307		
14.57698734			2.330150525		
15.64619516			2.511875588		
16.99146498			2.73958304		
18.75654664			3.037119197		
21.21792366			3.450310446		
25			4.082560777		

Appendix C

A.17 CYLINDER WITH MOONPOOL - TEST17 [21]

Input file: test17a.cfg

! TEST17A.CFG file, cylinder with moonpool, free lid

ipltdat=5

ilowgdf=5

ILOWHI=1

IALTFRC=2

ISOLVE=1

PANELSIZE = 0.2 (use default .spl parameters)

IPERIN=3 (input wavenumber)

IPEROUT=3 (output wavenumber)

ILOG=1

NUMHDR=1

IGENMDS=17

NEWMDS = 2

Input file: test17a.pot

TEST17 cylinder with moonpool, NPATCH=3

-1.

0 0 IRAD, IDIFF

NPERGROUP=3

-11

0.10 0.05 (end of group 1, K = 0.10 to 0.60)

-40

0.61 0.01 (end of group 2, K = 0.61 to 1.00)

-10

1.05 0.05 (end of group 3, K = 1.05 to 1.50)

1 NBETA (array BETA follows)

180.

1 NBODY

test17a.gdf

0. 0. 0. 0. XBODY

1 0 1 0 1 0 IMODE(1-6)

PICT PICT

Input file: test17a.gdf

TEST17a cylinder with moonpool – undamped patch on free surface

1. 9.80665 ULEN GRAV

1 1 ISX ISY

4 -7 NPATCH IGDEF

1 NLINES

0.5 1.0 0.25 radius, draft, moonpool radius

Input file: test17a.frc

TEST17a moonpool with generalized modes for free surface - no damping

1 1 1 1 0 0 0 0 0

1.

0. 0. 0.

1 imass (mass matrix of body)

0.589 0.0 0.0 0.0 0.0 0.0 0.0 0.0

0.0 0.589 0.0 0.0 0.0 0.0 0.0 0.0

0.0 0.0 0.589 0.0 0.0 0.0 0.0 0.0

0.0 0.0 0.0 0.147 0.0 0.0 0.0 0.0

0.0 0.0 0.0 0.0 0.147 0.0 0.0 0.0

0.0 0.0 0.0 0.0 0.0 0.147 0.0 0.0

0.0 0.0 0.0 0.0 0.0 0.0 0.0 0.0

0.0 0.0 0.0 0.0 0.0 0.0 0.0 0.0

0 idamp

0 istif

0

0

Appendix D

Calibrated input file: test17a.cfg

NOOUT= 1 1 0 1 0 0 0 0 0
ILOWHI=1
ILOWGDF=1
IPOTEN=1
IFORCE=1
IALTFRC=2
ISOLVE=1
PANEL_SIZE = 16 (use default .spl parameters)
! IPERIN=3 (input wavenumber)
! IPEROUT=3 (output wavenumber)
ILOG=1
NUMHDR=1
IGENMDS=17
NEWMDS = 2

Calibrated input file: test17a.pot

Floating dock
1000 HBOT
1 1 IRAD, IDFF
50 NPER (periods follow)
3 4 5 6 7 8 9 10 11 12
13 14 15 16 17 18 19 20 21 22
23 24 25 26 27 28 29 30 31 32
33 34 35 36 37 38 39 40 41 42
43 44 45 46 47 48 49 50 51 52
7 NBETA (directions follow)
0 30 60 90 120 150 180
1 NBODY

Draft80BoxR46.gdf

0. 0. 0. 0. XBODY(1-4)

1 1 1 1 1 1 IMODE(1-6)

Calibrated input file: test17a.frc

Floating dock

1 1 1 1 0 0 1 0 0 IOPTN(1-9)

1000 RHO

0 0 -55 VCG

1 IMASS

1.81583e+08 0 0 0 -9.98709e+09 0 0 0

0 1.81583e+08 0 9.98709e+09 0 0 0 0

0 0 1.81583e+08 0 0 0 0 0

0 9.98709e+09 0 6.89483e+11 0 0 0 0

-9.98709e+09 0 0 0 6.89483e+11 0 0 0

0 0 0 0 2.30046e+11 0 0

0 0 0 0 0 0 0

0 0 0 0 0 0 0

1 IDAMP

2e+07 0 0 0 0 0 0

0 0 0 0 0 0 0

0 0 2e+07 0 0 0 0

0 0 0 0 0 0 0

0 0 0 0 0 0 0

0 0 0 0 0 0 0

0 0 0 0 0 2e+05 0

0 0 0 0 0 0 0

1 ISTIF

0 0 0 0 0 0 0

0 0 0 0 0 0 0

0 0 0 0 0 0 0

00000000

00000000

00000000

00000000

00000000

0 NBETA

0 NFIELD (point coordinates follow)

Appendix E

	x_{max}	z_{max}	θ_{max}
1	0.852 m	0.063 m	1.08 deg
2	0.873 m	0.074 m	1.05 deg
3	0.893 m	0.078 m	1.07 deg
4	0.737 m	0.046 m	0.91 deg
5	0.836 m	0.056 m	1.00 deg
6	0.736 m	0.052 m	0.93 deg
7	0.806 m	0.051 m	0.95 deg
8	0.740 m	0.050 m	0.88 deg
9	0.895 m	0.048 m	1.09 deg
10	0.887 m	0.043 m	1.03 deg
MEAN	0.826 m	0.056 m	1.00 deg

Table 6.3: Results for wave condition: $H_s=2m$, $T_p=9s$

	x_{max}	z_{max}	θ_{max}
1	1.081 m	0.295 m	1.91 deg
2	1.193 m	0.326 m	1.80 deg
3	1.213 m	0.339 m	2.04 deg
4	1.174 m	0.293 m	1.86 deg
5	1.879 m	0.381 m	2.03 deg
6	1.164 m	0.392 m	1.70 deg
7	1.162 m	0.337 m	1.88 deg
8	1.195 m	0.354 m	1.69 deg
9	1.227 m	0.368 m	2.06 deg
10	1.437 m	0.382 m	2.01 deg
MEAN	1.273 m	0.347 m	1.90 deg

Table 6.4: Results for wave condition: $H_s=2m$, $T_p=13s$

	x_{max}	z_{max}	θ_{max}
1	1.277 m	0.140 m	1.62 deg
2	1.305 m	0.165 m	1.57 deg
3	1.336 m	0.172 m	1.59 deg
4	1.105 m	0.102 m	1.36 deg
5	1.249 m	0.122 m	1.50 deg
6	1.103 m	0.116 m	1.39 deg
7	1.204 m	0.112 m	1.41 deg
8	1.103 m	0.112 m	1.32 deg
9	1.340 m	0.106 m	1.63 deg
10	1.328 m	0.095 m	1.53 deg
MEAN	1.235 m	0.124 m	1.49 deg

Table 6.5: Results for wave condition: $H_s=3\text{m}$, $T_p=9\text{s}$

	x_{max}	z_{max}	θ_{max}
1	1.622 m	0.451 m	2.85 deg
2	1.775 m	0.496 m	2.69 deg
3	1.792 m	0.522 m	3.04 deg
4	1.758 m	0.438 m	2.78 deg
5	2.812 m	0.590 m	3.04 deg
6	1.751 m	0.570 m	2.54 deg
7	1.736 m	0.509 m	2.80 deg
8	1.787 m	0.543 m	2.53 deg
9	1.836 m	0.535 m	3.08 deg
10	2.141 m	0.574 m	3.01 deg
MEAN	1.901 m	0.523 m	2.84 deg

Table 6.6: Results for wave condition: $H_s=3\text{m}$, $T_p=13\text{s}$

	x_{max}	z_{max}	θ_{max}
1	5.629 m	2.921 m	10.00 deg
2	6.486 m	2.796 m	9.98 deg
3	6.264 m	2.969 m	10.77 deg
4	5.603 m	2.994 m	10.26 deg
5	5.500 m	3.223 m	11.38 deg
6	6.872 m	3.587 m	9.67 deg
7	5.685 m	3.131 m	10.06 deg
8	6.272 m	3.115 m	9.90 deg
9	6.014 m	3.422 m	12.57 deg
10	7.467 m	3.766 m	10.51 deg
MEAN	6.179 m	3.192 m	10.51 deg

Table 6.7: Results for wave condition: $H_s=11\text{m}$, $T_p=14.2\text{s}$

